

Relativistic unitary description of $\pi\pi$ scattering

M. A. Pichowsky, A. Szczepaniak, and J. T. Londergan

Department of Physics and Nuclear Theory Center, Indiana University, Bloomington, Indiana 47405

A framework for the study of hadron scattering based on the Bakamjian-Thomas construction of relativistic quantum mechanics is introduced. The unitary framework describes the relativistic coupled-channel scattering of one-, two- and three-body states for finite-sized hadrons of any spin and at all energies. The utility of the approach is demonstrated in a preliminary study of two-pion scattering from threshold to 1400 MeV. The framework provides an excellent description of the available data for S - and P -wave $\pi\pi$ scattering phase shifts and inelasticities. Numerical methods are described and shown to maintain the unitarity of the approach to better than one part per million.

I. INTRODUCTION

We present a nonperturbative framework capable of describing the relativistic, coupled-channel scattering of hadrons. The approach is based on a relativistic Hamiltonian formulation with model interactions introduced into the mass operator, and with few-body states implemented in a way that maintains the unitarity of the theory. The elementary degrees of freedom in the framework are finite-sized hadrons which provide a natural ultraviolet regularization, ensuring that the scattering amplitudes are finite.

The Hilbert space is truncated to a finite number of states. Here, only one-, two- and three-body states are retained in the Hilbert space, however, states of higher particle-numbers can be included in a straightforward manner. A central and novel feature of this framework is the explicit inclusion of both real and imaginary parts of scattering amplitudes arising from the opening of three-body channels. The proper handling of three-body unitarity cuts is crucial to gaining a deeper understanding of several well-known scattering systems; a good example is the πN scattering in the P_{11} channel, which exhibits a significant inelasticity arising from the intermediate three-body $\pi\pi N$ state [1].

It presents a formidable challenge to develop a generalized, relativistic scattering framework to describe the final-state interactions between hadrons, that includes the effects of three-body unitarity cuts. Nonetheless, a practical framework which can treat hadron reactions beyond the lowest-order valence quark picture is clearly desirable. For example, the systematic analysis of hadron reactions in the baryon resonance region currently being conducted in Hall B at the Thomas Jefferson National Accelerator Facility (TJNAF) requires that such a framework be used to extract information about baryon resonances in this highly complex dynamical region. The

framework developed herein is an attempt to construct a useful, relativistic framework capable of describing the nonperturbative, low-momentum transfer final-state interactions between hadrons in a unitary manner.

For the first application of the framework developed here, we introduce a simple model for $\pi\pi$ scattering in the S and P partial waves for energies ranging from the two-pion threshold up to 1400 MeV. This system provides an excellent test for our framework. A relativistic treatment is quite important when dealing with particles as light as pions, as the interplay between strong dynamics and chiral symmetry makes this system quite interesting. The $\pi\pi$ system is somewhat simpler than others, in that its study requires only a minimal complication from the proper implementation of relativistic spins, since both of the two-body states ($\pi\pi$ and $K\bar{K}$) involved are comprised of spin-0 particles. Finally, a nice aspect of applying the framework to $\pi\pi$ scattering is the relative wealth of experimental data for, and current interest in $\pi\pi$ scattering, particularly in the isoscalar, S -wave channel.

One drawback with using $\pi\pi$ scattering as our touchstone may be that inelasticities due to *open* states of three or more particles, do not appear to be significant for this process in particular; that is, the $\rho\pi\pi$ and $\pi\pi\pi\pi$ thresholds seem to have little impact on the S - and P -wave observables. The effects of these open channels that one expects to observe, seem to be overwhelmed by the opening of the $K\bar{K}$ channel. Nonetheless, several important aspects of the framework can be explored in an application to $\pi\pi$ scattering.

The isoscalar-scalar ($I = 0, J^{PC} = 0^{++}$) channel of $\pi\pi$ scattering has been a subject of numerous and extensive studies. The study of meson scattering in this low-energy region may be an ideal test of our understanding of the interplay between bound states in QCD and chiral dynamics. The region near $E = 1000$ MeV is perhaps most interesting, as it is dominated by the mixing between $\pi\pi$ and $K\bar{K}$ channels and the scalar $f_0(980)$ meson resonance. The nature of the $f_0(980)$ resonance, and the question of whether it is comprised of valence quarks or arises purely from meson scattering dynamics, has been addressed by many authors [2–8]. Above this energy region, three additional scalar meson resonances have been well established. These are referred to as the $f_0(1370)$, $f_0(1500)$ and the $f_0(1710)$. It is still unclear which of these should be considered as quark-antiquark bound states, glueballs or possibly resonances arising from dynamical effects of final-state interactions [9–13]. Thus, the isoscalar-scalar channel remains a source of great interest and mystery for meson phenomenology.

Although there have been previous studies which em-

ploy a framework similar to the one developed here, there are some important differences. Most studies of meson scattering dynamics are based on potential models (as is the framework developed here.) However, most other approaches typically include one- and two-particle channels only; that is, they include s -channel states and perhaps several two-particle channels, such as $\pi\pi$, $K\bar{K}$, $\sigma\sigma$, etc. They either neglect the possibility of open three-particle channels altogether or only partially implement them. For example, in the model developed by the Julich group [14], the interaction potentials between two-particle channels, such as $\pi\pi$ - $\pi\pi$ or $\pi\pi$ - $K\bar{K}$ interactions are obtained using an instantaneous approximation of a meson-exchange model. Such instantaneous approximations generally do not account for absorptive effects due to the opening of three-body channels. Still, there is no question that the Julich model quite successfully describes the phase shifts and inelasticities of $\pi\pi$ scattering for S , P and D waves. Alternatively, the Krakow group [15] has developed a separable-potential model for $\pi\pi$ scattering. In their calculation, few-body dynamical effects are incorporated by including additional, *effective* two-body channels, such as a $\sigma\sigma$ channel [16]. Their model also obtains excellent results for the $\pi\pi$ phase shifts and inelasticities.

The outline of this article is as follows. In Sec. II, we briefly construct the relativistic scattering formalism employed herein. We begin with a short proof of covariance of observables calculated within the framework, and then provide a brief derivation of the formal solution of the Lippmann-Schwinger scattering equations, and describe the truncation of the Hilbert space necessary to obtain the closed-form solution. We solve the T -matrix elements for one-body to one-body transitions and then derive the integral equations for the two- and three-body scattering equations. The section concludes with a summary of the dynamical assumptions and restrictions implemented in our calculations.

In Sec. III, the coupled Lippmann-Schwinger equations, derived in Sec. II, are solved by expanding them in a partial-wave basis and writing them in terms of the relative and center-of-momentum (CM) coordinates. A review of how the two- and three-body states are boosted from their CM frame to the laboratory frame is provided, and explicit forms for the various potential matrix elements are given. Following this, one- and two-body self-energies are calculated, and the numerical techniques used to solve the resulting integral equations for scattering amplitudes are outlined.

Finally, the unitarity of the framework is discussed in detail. It is shown that the incoming particle flux can be observed in the outgoing one-body, two-body and three-body channels. In our $\pi\pi$ scattering model, this is calculated explicitly as a test of unitarity and of the numerical methods employed. It is argued that there are two possible sources of unitarity violation. The first is due to numerical errors, in particular round-off errors, and the use of a finite mesh size. The second violation arises because

of the use of a finite value of the “adiabatic switching parameter” ϵ used to regulate poles which occur in our formalism. It is shown that, in practice, ϵ can always be chosen small enough so that its contribution to unitarity violations is negligible. Then, one observes that the numerical methods employed herein maintain the unitarity of the framework to better than one part in a million. It is in this sense that we claim our approach is *effectively unitary*.

In Sec. IV, our framework is first applied to a study of $\pi\pi$ scattering. The particle states that are included in the model are discussed, along with the necessary dynamical model parameters. The interactions employed in this study arise from the meson exchanges which couple states of various numbers of particles to each other. In our framework, these interactions arise from one-, two- and three-meson intermediate states which may exhibit production thresholds, resulting in absorptive contributions to the kernels and self-energies appearing in the Lippmann-Schwinger equations. A simple fitting procedure is shown to provide excellent agreement with data for $\pi\pi$ scattering phase shifts and inelasticities. We discuss in detail the relevant model dynamics that produce the various features observed in the resulting phase shifts and inelasticities. Finally, in Sec. V, the article is summarized and plans for future studies are presented.

II. FORMALISM

In this section, a relativistic Hamiltonian framework is developed that provides a covariant unitary approach to the study of multichannel scattering. Lorentz symmetry is maintained by identifying the interactions with the mass operator (that is, the Hamiltonian in the center-of-momentum frame). It is shown in Ref. [17] that the complete set of Poincare generators can be constructed in a simple way that separates the internal dynamics from the center-of-momentum (CM) motion. It was shown by Betz and Coester [18] that such a framework can satisfy cluster separability. Both of these are necessary features for the study of hadron scattering within a relativistic, quantum mechanical framework.

In Sec. II A, the Lorentz covariance of the framework is demonstrated and the mass operator \mathcal{M} is constructed. It is shown that this framework leads to Lorentz-invariant on-shell T -matrix elements $T(E, \mathbf{P})$ for colliding particles with total momentum \mathbf{P} and energy E ; that is, one finds $T(E, \mathbf{P}) = T(\sqrt{s})$ where $\sqrt{s} = \sqrt{E^2 - \mathbf{P}^2}$ is the invariant mass of the system.

The next step is to truncate the Hilbert space to include only those channels which are essential to describe the scattering system of interest within a particular energy range. In Sec. II B, the Hilbert space is truncated to contain only one-, two- and three-particle states. Following this truncation, the operator form of the Lippmann-Schwinger equation can be written as a set of coupled

integral equations. The input that determines the dynamics is given in terms of model potential matrix elements. Once these are provided, the full scattering problem is solved in a straightforward manner. In Sec. II C, the constraints of the framework are summarized.

A. Relativistic covariance

A simple realization of the Poincare algebra for an interacting system of a finite number of constituents is given by the Bakamjian-Thomas construction [17]. This approach has the advantage of providing a Lorentz-covariant generalization for a large class of noncovariant microscopic models, such as the constituent quark model. In principle, a noncovariant microscopic model could be used to obtain the underlying elementary meson-meson potentials which determine the scattering interactions. In this case, one might consider this framework as a means to extend the original noncovariant model dynamics, allowing for a Lorentz-covariant treatment of scattering phenomena.

The explicit construction of the Poincare algebra proceeds as follows. Starting from a system of *noninteracting* particles, described by their coordinates \mathbf{x}_a , momenta \mathbf{p}_a , spins \mathbf{s}_a , and masses m_a , the Poincare generators are

$$\begin{aligned} H &= \sum_a \mathcal{E}(m_a, \mathbf{p}_a) = \sum_a \sqrt{m_a^2 + \mathbf{p}_a^2}, \\ \mathbf{P} &= \sum_a \mathbf{p}_a, \\ \mathbf{J} &= \sum_a \mathbf{x}_a \times \mathbf{p}_a + \mathbf{s}_a, \\ \mathbf{K} &= \sum_a \frac{1}{2} \{ \mathbf{x}_a, \mathcal{E}(m_a, \mathbf{p}_a) \} - \frac{\mathbf{s}_a \times \mathbf{p}_a}{\mathcal{E}(m_a, \mathbf{p}_a) + m_a}. \end{aligned} \quad (2.1)$$

Here, H and \mathbf{P} are the total free energy and linear momentum of the system, \mathbf{J} and \mathbf{K} are the total angular momentum and boost operators, respectively. The relative coordinates \mathbf{r}_a , relative momenta \mathbf{k}_a , center-of-momentum (CM) spins \mathbf{s}'_a , and the CM coordinates \mathbf{R}_{cm} , total momentum \mathbf{P}_{cm} , and total spin \mathbf{S}_{cm} , are introduced via the Gartenhaus-Schwartz transformation which allows a separation of the *internal* dynamics and CM motion. In terms of these new variables, the Poincare generators are given by

$$\begin{aligned} H &= \sqrt{\mathbf{P}^2 + \mathcal{M}^2(\mathbf{k}_1, \mathbf{k}_2, \dots)}, \\ \mathbf{P} &= \mathbf{P}_{cm}, \\ \mathbf{J} &= \mathbf{R}_{cm} \times \mathbf{P}_{cm} + \mathbf{S}_{cm}, \\ \mathbf{K} &= \frac{1}{2} \{ \mathbf{R}_{cm}, H \} - \frac{\mathbf{S}_{cm} \times \mathbf{P}_{cm}}{H + \mathcal{M}(\mathbf{k}_1, \mathbf{k}_2, \dots)}, \end{aligned} \quad (2.2)$$

with the constraints,

$$\sum_a m_a \mathbf{r}_a = 0,$$

$$\begin{aligned} \sum_a \mathbf{k}_a &= 0, \\ \mathbf{S}_{cm} - \left(\sum_a \mathbf{r}_a \times \mathbf{k}_a + \mathbf{s}'_a \right) &= 0. \end{aligned} \quad (2.3)$$

In Eq. (2.2), the quantity $\mathcal{M} = \mathcal{M}(\mathbf{k}_1, \mathbf{k}_2, \dots)$ is referred to as the *free* invariant mass in the Schrödinger picture. The internal momenta \mathbf{k}_a are related to the individual particle momenta \mathbf{p}_a via a free Lorentz transformation to the CM frame,

$$\begin{aligned} \mathbf{k}_a &= \Lambda(\mathbf{k}_a \leftarrow \mathbf{p}_a) \mathbf{p}_a \\ &= \mathbf{p}_a + \frac{\mathbf{p}_a \cdot \mathbf{P}}{\mathcal{M}(\mathcal{M} + H)} \mathbf{P} - \frac{\mathcal{E}(m_a, \mathbf{p}_a)}{\mathcal{M}} \mathbf{P} \end{aligned} \quad (2.4)$$

and the CM frame spins \mathbf{s}'_a are related to the individual spins \mathbf{s}_a via a Wigner rotation corresponding to the product of Lorentz boosts $R = \Lambda(0 \leftarrow \mathbf{p}_a) \Lambda(\mathbf{p}_a \leftarrow \mathbf{k}_a) \Lambda(\mathbf{k}_a \leftarrow 0)$, leading to

$$\mathbf{s}'_a = D^{(s)}(R) \mathbf{s}_a D^{(s)}(R)^*. \quad (2.5)$$

Interactions are incorporated into the Poincare generators by the addition of a term in the free mass operator,

$$\mathcal{M} \rightarrow \mathcal{M}_I(\mathbf{r}_a, \mathbf{k}_a, \mathbf{s}'_a) = \mathcal{M} + V. \quad (2.6)$$

Thus, transforming the free Hamiltonian H into the interacting Hamiltonian H_I ,

$$\begin{aligned} H &\rightarrow H_I = H + W, \\ W &= \sqrt{\mathcal{M}_I^2 + \mathbf{P}^2} - \sqrt{\mathcal{M}^2 + \mathbf{P}^2}. \end{aligned} \quad (2.7)$$

This replacement preserves the canonical commutation relations, provided $V = V(\mathbf{r}_a, \mathbf{k}_a, \mathbf{s}'_a)$ is a function of internal coordinates only and is invariant under rotations $[V, \mathbf{J}] = [V, \mathbf{S}_{cm}] = 0$. For example, consider the case for which the elementary interaction is a Yukawa-type three-meson vertex. The matrix elements of the three-meson interaction vertex would be given by $\langle a|V|bc \rangle$ and would only depend on the internal variables associated with the CM frame where $\mathbf{p}_a = \mathbf{p}_b + \mathbf{p}_c = 0$. Of course, these internal variables can be expressed in terms of the individual particle momenta in another frame by using the boost relations analogous to Eqs. (2.4) and (2.5).

Within this framework, the Lorentz covariance of observables may be demonstrated from the following considerations. Construct an invariant \mathcal{T} -matrix which satisfies a *Lorentz-invariant* Lippmann-Schwinger equation (LSE),

$$\mathcal{T} = \mathcal{V} + \mathcal{V} \mathcal{G} \mathcal{T}, \quad (2.8)$$

with an invariant interaction \mathcal{V} ,

$$\begin{aligned} \mathcal{V} &= H_I^2 - H^2 \\ &= (\mathbf{P}^2 + \mathcal{M}_I^2) - (\mathbf{P}^2 + \mathcal{M}^2) \\ &= W^2 + HW + WH \\ &= V^2 + \mathcal{M}V + V\mathcal{M}, \end{aligned} \quad (2.9)$$

and an invariant propagator \mathcal{G} for scattering energy E , given by

$$\begin{aligned}\mathcal{G} &= (E^2 - H^2 + i\epsilon)^{-1} \\ &= (E^2 - \mathbf{P}^2 - \mathcal{M}^2 + i\epsilon)^{-1}.\end{aligned}\quad (2.10)$$

Since \mathcal{V} is independent of the CM momentum \mathbf{P} and the scattering energy E , one may rewrite the scattering energy $E = \sqrt{s + \mathbf{P}^2}$, in terms of a new variable s , referred to as the invariant mass squared. Noting, from Eq. (2.10), that the propagator $\mathcal{G}(s)$ is a function of the invariant mass squared only, one concludes that the LSE (2.8) depends only on the invariant mass squared s . It follows that the resulting \mathcal{T} -matrix, $\mathcal{T}(\sqrt{s})$ depends only on the invariant mass squared s .

It is possible to relate the *on-shell* matrix elements of this invariant \mathcal{T} -matrix to the *on-shell* matrix elements of a T -matrix that is the solution of a non-invariant LSE with the interaction potential W ,

$$T(E, \mathbf{P}) = W + W G(E) T(E, \mathbf{P}), \quad (2.11)$$

where $G(E) = (E - H + i\epsilon)^{-1}$. The relation between the on-shell matrix elements is given by

$$\mathcal{T}(\sqrt{s}) = 2\sqrt{s + \mathbf{P}^2} T(E, \mathbf{P}), \quad (2.12)$$

which can be demonstrated term by term by expanding the *on-shell* matrix elements of \mathcal{T} in powers of the potential V ,

$$\begin{aligned}\mathcal{T} &= \mathcal{V} + \mathcal{V}\mathcal{G}(E)\mathcal{V} + O(V^3) \\ &= W^2 + 2EW \\ &\quad + W(E + H) \frac{1}{E^2 - H^2 + i\epsilon} (E + H)W + O(V^3) \\ &= 2EW + 2EW \frac{1}{E - H + i\epsilon} W + O(V^3) \\ &= 2ET(E, \mathbf{P}).\end{aligned}$$

In this article, we choose to work in the CM frame where $E = \sqrt{s}$, then the interaction potential $W = \mathcal{M}_I - \mathcal{M} = V$, and the relevant LSE is

$$T(E) = V + V G(E) T(E). \quad (2.13)$$

For the arguments above, one observes that in the CM frame,

$$\mathcal{T}(\sqrt{s}) = 2\sqrt{s} T(\sqrt{s}). \quad (2.14)$$

Thus, the on-shell matrix elements of the solution $T(E = \sqrt{s})$ of the non-invariant LSE in Eq. (2.13) are related by Eq. (2.14) to the on-shell matrix elements of the solution $\mathcal{T}(\sqrt{s})$ of the invariant LSE of Eq. (2.8). It follows that observables calculated from Eq. (2.13) are equivalent to those calculated from a Lorentz-invariant theory.

B. Formal solution of the Lippmann-Schwinger Equation

In the framework for relativistic scattering outlined above, the particle dynamics are given in the center of momentum (CM) frame where $\mathbf{P} = 0$ by the invariant mass operator,

$$\mathcal{M}_I = \mathcal{M} + V. \quad (2.15)$$

The quantity \mathcal{M} , introduced in Eq. (2.2), is the *free* invariant mass in the Schrödinger picture and V is the elementary interaction potential. To the latter, a slowly-varying time-dependence is added,

$$V \rightarrow V e^{-\epsilon|t|}. \quad (2.16)$$

The characteristic time-scale is $1/\epsilon$, where $\epsilon > 0$ is referred to as the *adiabatic switching scale*. This time-dependent potential produces an invariant mass \mathcal{M}_I in Eq. (2.15) which is also time dependent. Of course, such a time dependence violates the unitarity of the theory. The magnitude of the violation is proportional to the small adiabatic switching scale ϵ . Hence, one requires that the value of ϵ be much smaller than any of the physical energy scales of interest. In Sec. III E, the role of ϵ in numerical computations is explored and the ϵ dependence of the unitarity relations is explicitly calculated.

In the interaction picture the initial system is prepared in an eigenstate $|\alpha\mathbf{P}\rangle$ of the total momentum \mathbf{P} at asymptotically early times $t \rightarrow -\infty$. Here, α denotes all other quantum numbers necessary to uniquely determine the state. At a later time $t \rightarrow +\infty$, the final state $|\beta\mathbf{Q}\rangle$ is observed. Since the time-dependent potential in Eq. (2.16) vanishes for large asymptotic times t , it follows that the initial and final states may be taken to be eigenstates of the *free* invariant mass \mathcal{M} with eigenvalues \mathcal{M}_α and \mathcal{M}_β , respectively.

The probability amplitude for observing the final state $|\beta\mathbf{Q}\rangle$, given an initial state $|\alpha\mathbf{P}\rangle$, is given by the S -matrix element $\langle\beta\mathbf{Q}|S(E)|\alpha\mathbf{P}\rangle$. The T -matrix $T(E, \mathbf{P})$ is defined by the Lippmann-Schwinger equation (LSE) of Eq. (2.13) and determines the on-shell S -matrix elements,

$$\begin{aligned}\langle\beta\mathbf{Q}|S(E)|\alpha\mathbf{P}\rangle &= \langle\beta\mathbf{Q}|\alpha\mathbf{P}\rangle \\ &\quad - 2\pi i \delta(\mathcal{E}(\mathcal{M}_\beta, \mathbf{Q}) - \mathcal{E}(\mathcal{M}_\alpha, \mathbf{P})) \langle\beta\mathbf{Q}|T(E, \mathbf{P})|\alpha\mathbf{P}\rangle,\end{aligned}\quad (2.17)$$

where $\mathcal{E}(\mathcal{M}_\alpha, \mathbf{P}) = \sqrt{\mathcal{M}_\alpha^2 + \mathbf{P}^2}$.

The potential V and the T -matrix describe all interactions between the various channels, including channels with differing numbers of particles. In general, they do not conserve particle number. Therefore, the LSE of Eq. (2.13) represents an countably infinite system of coupled-channel equations which couple states of different numbers of particles.

This infinite system of coupled equations may be simplified by truncating the Hilbert space to include only a

finite number of states that are expected to contribute substantially to a given reaction. For the purposes of this study, the Hilbert space is restricted to contain a finite number of one-, two-, and three-particle states. Furthermore, the particles are assumed to be of finite spatial extension, thereby providing an ultraviolet regularization to the theory. With these restrictions, the LSE of Eq. (2.13) reduces to a closed system of integral equations which may be solved exactly. The addition of states with a higher number of particles, such as four-particle states, can in principle be included in a straightforward manner but the resulting set of equations would be far more complicated than the set studied here.

The main objective of this work is to develop a framework for handling up to three-body channels in a fully unitary fashion, by including effects beyond their contribution to the real part of effective, two-body potentials. The intended application of the framework is to provide a description of soft final-state interactions in hadron production processes. Such processes are distinguished by their strong couplings and low momentum transfers. For this reason, we choose to employ the composite hadrons (mesons and/or baryons) rather than quarks as the fundamental degrees of freedom.

The truncation of the Hilbert space to contain only one-, two- and three-hadron states may be sufficient since, in many applications, states with higher numbers of hadrons contribute less to two-hadron elastic scattering amplitudes than states with fewer hadrons. This suppression arises because many-hadron intermediate states typically have a large invariant mass, which appears in the denominator of their Green function G . This tends to weaken the state's contribution. Thus, one might expect that such a truncation scheme, which neglects states with four or more hadrons, could provide a reasonable description of the residual strong interactions between mesons and baryons, for scattering energies which are below the energies of typical four-hadron intermediate states.

The matrix elements of the potential V describe the couplings between hadrons that arise from an underlying QCD dynamics of quarks and gluons. Color confinement requires that all physical particle thresholds are associated with the colorless hadron states. It follows that the matrix elements of V are real. In this framework, all of the analytic structure of the T -matrix necessarily arises from the color-singlet hadron poles and branch cuts which result from the LSE of Eq. (2.13).

Once the Hilbert space has been truncated to include only one-, two- and three-particle states, Eq. (2.13) may be expanded and rewritten in a simpler form by labeling each of the Hilbert space operators with subscripts indicating the numbers of particles they act on. The potential V is of the form

$$V = \begin{pmatrix} V_{11} & V_{12} & V_{13} \\ V_{21} & V_{22} & V_{23} \\ V_{31} & V_{32} & V_{33} \end{pmatrix}. \quad (2.18)$$

For example, the part of the potential associated with

$$V = \begin{pmatrix} \text{---}\times\text{---} & \text{---}\cup\text{---} & 0 \\ \text{---}\cup\text{---} & \text{---}\times\text{---} + \text{---}\cap\text{---} & \text{---}\cup\text{---} + \text{---}\cap\text{---} \\ 0 & \text{---}\cup\text{---} + \text{---}\cap\text{---} & 0 \end{pmatrix}$$

FIG. 1. Schematic diagram of the interaction potential matrix V of Eq. (2.19).

the coupling of a one-particle state to a two-particle final state is denoted V_{21} . The resulting system of integral equations can be solved formally in a straightforward manner. The remainder of this section is devoted to a summary of the solution of the LSEs.

It is important to note that each matrix element of the potential V given schematically in Eq. (2.18) is itself a matrix, since it may contain interactions between any number of different particle channels. That is, matrix elements of the form V_{21} describe the couplings of any one-particle state with any two-particle state. The number of one-, two-, and three-particle states one wishes to include depends on the relevant particle channel states for a specific calculation.

For the application to $\pi\pi$ scattering considered in Sec. IV, a further simplification is made by assuming an absence of fundamental interactions in V that connect one-particle states to three-particle states, and a lack of interactions that directly connect three-particle states to three-particle states. Then, the potential V takes a simpler form,

$$V = \begin{pmatrix} V_{11} & V_{12} & 0 \\ V_{21} & V_{22} & V_{23} \\ 0 & V_{32} & 0 \end{pmatrix}. \quad (2.19)$$

The resulting potential V is shown schematically in Fig. 1.

The neglected terms $V_{13} = V_{31}^\dagger$ are associated with energy-independent transitions between one-particle and three-particle states. When such terms are neglected the only way in which a one-body state can decay into a three-body state is through a multiple-step process involving a two-body intermediate state.

In setting the term $V_{33} = 0$, several possible elementary interactions have been neglected. First, V_{33} describes direct energy-independent couplings between two three-body states, as well as interactions in which two of the particles interact while the third particle is a spectator. Such terms may be important. One might argue that it is inconsistent to include direct two-body interactions in V_{22} , but neglect the analogous two-body (plus spectator) interactions in V_{33} . Nonetheless, in this work such terms are ignored. The significance and role of these interactions will be addressed in future studies.

In the truncated Hilbert space, the free Green function is a diagonal matrix

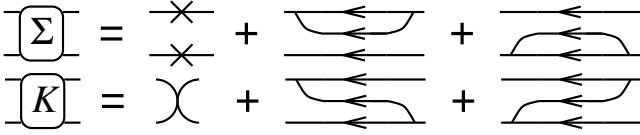


FIG. 2. Schematic diagram of the two-particle self-energy Σ , and the two-particle kernel K , as defined in Eq. (2.26).

$$G = \begin{pmatrix} G_1 & 0 & 0 \\ 0 & G_2 & 0 \\ 0 & 0 & G_3 \end{pmatrix}, \quad (2.20)$$

and the T -matrix is

$$T = \begin{pmatrix} T_{11} & T_{12} & T_{13} \\ T_{21} & T_{22} & T_{23} \\ T_{31} & T_{32} & T_{33} \end{pmatrix}. \quad (2.21)$$

In the CM frame, each submatrix G_1 , G_2 or G_3 in Eq. (2.20) is itself diagonal since our hadron states form a complete, orthogonal set of eigenstates of the free invariant mass operator \mathcal{M} .

Upon insertion of these forms for V , G and T from Eqs. (2.19), (2.20) and (2.21) into the LSE (2.13), one may formally solve this system of integral equations. The formal solution is the subject of the remainder of this section, while a discussion of the numerical solution is delayed until Sec. III.

1. Solution of the T -Matrix in the One-Particle Sector

In the following, the formal solution of the coupled Lippmann-Schwinger equation (LSE), is solved by first focusing on the one-particle sector and obtaining closed-form expressions for the one-particle T -matrix elements T_{11} , T_{12} and T_{13} . Then, the formal solutions for the two- and three-particle T -matrix elements are obtained.

First, consider the LSE for the one-particle T -matrix amplitudes T_{11} , T_{21} and T_{31} . These appear in the first column of Eq. (2.21) and are given by the following system of coupled integral equations:

$$T_{11} = V_{11} + V_{11}G_1T_{11} + V_{12}G_2T_{21} \quad (2.22)$$

$$T_{21} = V_{21} + V_{21}G_1T_{11} + V_{22}G_2T_{21} + V_{23}G_3T_{31} \quad (2.23)$$

$$T_{31} = V_{32}G_2T_{21}. \quad (2.24)$$

Substitution of Eq. (2.24) into Eq. (2.23) gives

$$\begin{aligned} T_{21} &= V_{21} + V_{21}G_1T_{11} \\ &\quad + (V_{22}G_2 + V_{23}G_3V_{32}G_2) T_{21}, \\ T_{21} &= [1 - (V_{22}G_2 + V_{23}G_3V_{32}G_2)]^{-1} \\ &\quad \times (V_{21} + V_{21}G_1T_{11}). \end{aligned} \quad (2.25)$$

The combination of terms $V_{22} + V_{23}G_3V_{32}$ in Eq. (2.25) appears frequently in the following derivations. These terms play an important role in the framework and so are collected and rewritten as the sum of Σ and K ,

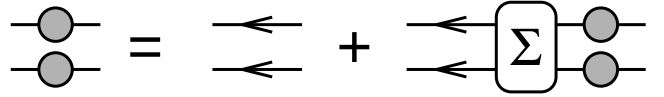


FIG. 3. Schematic diagram of the integral equation for the dressed two-body Green function \tilde{G}_2 given in Eq. (2.29).

$$\Sigma + K \equiv V_{22} + V_{23}G_3V_{32}. \quad (2.26)$$

These are referred to as the *two-particle self-energy* Σ , and the *two-particle kernel* K . The two terms are uniquely defined such that the matrix elements of the two-particle self-energy Σ contain only those terms proportional to a δ -function in the *relative* momentum of the two-particle state. Consequently, matrix elements of the two-particle kernel K contain all contributions that are *not* proportional to a δ -function in the relative momentum.

The two-particle self-energy and kernel are depicted schematically in Fig. 2. In the following, it will become apparent that Σ and K are the central elements of the framework, from which all other quantities are obtained. It will also turn out that *all* effects due to three-particle intermediate states can be traced back to these two amplitudes.

Substituting the relations of Eqs. (2.24) and (2.25) into Eq. (2.22) gives the closed-form integral equation for T_{11} ,

$$\begin{aligned} T_{11} &= V_{11} + V_{11}G_1T_{11} \\ &\quad + V_{12}G_2[1 - (V_{22}G_2 + V_{23}G_3V_{32}G_2)]^{-1} \\ &\quad \times (V_{21} + V_{21}G_1T_{11}), \\ &= (V_{11} + V_{12}G_2(G_2^{-1} - \Sigma - K)^{-1}V_{21}) (1 + G_1T_{11}), \\ &= (V_{11} + V_{12}\tilde{G}_2(1 - K\tilde{G}_2)^{-1}V_{21}) (1 + G_1T_{11}), \end{aligned} \quad (2.27)$$

where the *dressed* two-particle Green function

$$\tilde{G}_2 = (G_2^{-1} - \Sigma)^{-1}, \quad (2.28)$$

was introduced. The dressed two-particle Green function \tilde{G}_2 satisfies the integral equation,

$$\tilde{G}_2 = G_2 + G_2 \Sigma \tilde{G}_2, \quad (2.29)$$

shown schematically in Fig. 3. The role played by the two-particle self-energy Σ in the expression for the dressed two-particle Green function of Eqs. (2.28) and (2.29) justifies its nomenclature.

The closed-form expression for the one-particle to one-particle scattering matrix element T_{11} is

$$T_{11} = (V_{11} + V_{12}\tilde{G}_2\tilde{V}_{21})(1 + G_1T_{11}) \quad (2.30)$$

and its formal solution is

$$T_{11} = G_1^{-1}\tilde{G}_1\Pi. \quad (2.31)$$

In Eq. (2.31), we have introduced the quantities

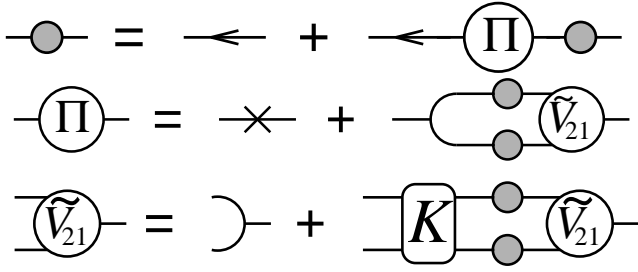


FIG. 4. Schematic diagram of the integral equations for the dressed one-body Green function \tilde{G}_1 , the one-body self-energy Π , and the dressed vertex \tilde{V}_{21} . These diagrams depict the expressions in Eqs. (2.32), (2.33) and (2.34).

$$\tilde{G}_1 = (G_1^{-1} - \Pi)^{-1}, \quad (2.32)$$

$$\Pi = V_{11} + V_{12}\tilde{G}_2\tilde{V}_{21}, \quad (2.33)$$

$$\begin{aligned} \tilde{V}_{21} &= V_{21} + K\tilde{G}_2\tilde{V}_{21}, \\ &= (1 - K\tilde{G}_2)^{-1}V_{21}, \end{aligned} \quad (2.34)$$

these are referred to as the *dressed* one-body Green function \tilde{G}_1 , the one-body self-energy Π , and the *dressed* vertex \tilde{V}_{21} . These quantities are shown schematically in Fig. 4.

The solutions for T_{21} and T_{31} are obtained in analogous manner,

$$\begin{aligned} T_{21} &= (1 - \Sigma G_2 - K G_2)^{-1}V_{21}(1 + G_1 T_{11}) \\ &= G_2^{-1}(\tilde{G}_2^{-1} - K)^{-1}V_{21}(1 + \tilde{G}_1 \Pi) \\ &= G_2^{-1}\tilde{G}_2(1 - K\tilde{G}_2)^{-1}V_{21}\tilde{G}_1(\tilde{G}_1^{-1} + \Pi) \\ T_{21} &= G_2^{-1}\tilde{G}_2\tilde{V}_{21}\tilde{G}_1 G_1^{-1} \end{aligned} \quad (2.35)$$

and

$$T_{31} = V_{32}\tilde{G}_2\tilde{V}_{21}\tilde{G}_1 G_1^{-1}. \quad (2.36)$$

The appearance of the terms $\tilde{G}G^{-1}$ in Eqs. (2.31), (2.35) and (2.36) is associated with the wavefunction renormalization. We discuss the role of wavefunction renormalization in Sec. III.

2. Solution of the T -Matrix in the Two-Particle and Three-Particle Sectors

The two-particle to two-particle scattering amplitude T_{22} is obtained by formally solving the system of coupled equations,

$$T_{12} = V_{12} + V_{11}G_1T_{12} + V_{12}G_2T_{22} \quad (2.37)$$

$$T_{22} = V_{22} + V_{21}G_1T_{12} + V_{22}G_2T_{22} + V_{23}G_3T_{32}, \quad (2.38)$$

$$T_{32} = V_{32} + V_{32}G_2T_{22}. \quad (2.39)$$

These coupled equations are solved in much the same way as the scattering matrix in the one-particle sector, although a detailed derivation of the solution is somewhat

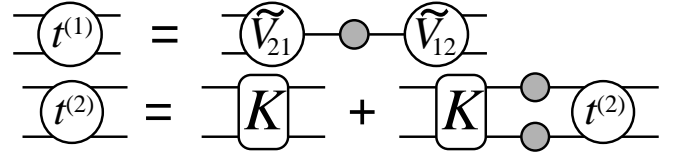


FIG. 5. Schematic diagram of the scattering amplitudes $t^{(1)}$ and $t^{(2)}$ which enter into the two-particle scattering matrix elements. These diagrams depict the expressions in Eqs. (2.41) and (2.42).

lengthy and is not presented here. The solution for the two-particle scattering T -matrix can be written as

$$T_{22} = G_2^{-1}\tilde{G}_2(t^{(1)} + t^{(2)})\tilde{G}_2G^{-1} + G_2^{-1}\tilde{G}_2\Sigma, \quad (2.40)$$

where

$$t^{(1)} = \tilde{V}_{21}\tilde{G}_1\tilde{V}_{12}, \quad (2.41)$$

$$\begin{aligned} t^{(2)} &= K + K\tilde{G}_2t^{(2)}, \\ &= (1 - K\tilde{G}_2)^{-1}K. \end{aligned} \quad (2.42)$$

These two scattering amplitudes are shown schematically in Fig. 5. Briefly, the contributions to the two-body scattering amplitude T_{22} that proceed through one-body channels are denoted $t^{(1)}$, while contributions that don't proceed through one-body channels are denoted $t^{(2)}$. Both $t^{(1)}$ and $t^{(2)}$ contain the effects of the two- and three-body singularities, but only $t^{(1)}$ contains one-body singularities.

The only remaining T -matrices necessary for a complete solution of the LSE of Eq. (2.13) are T_{23} and T_{33} . These are obtained by expanding the LSE using Eqs. (2.19), (2.20) and (2.21), and noting that $V_{13} = V_{31} = 0$. One then obtains

$$T_{13} = V_{11}G_1T_{13} + V_{12}G_2T_{23}, \quad (2.43)$$

$$T_{23} = V_{23} + V_{21}G_1T_{13} + V_{22}G_2T_{23} + V_{23}G_3T_{33}, \quad (2.44)$$

$$T_{33} = V_{32}G_2T_{23}. \quad (2.45)$$

Clearly, T_{33} is easy to obtain once T_{23} is known. Therefore, one need only focus on deriving a closed-form expression for T_{23} . The solution of Eq. (2.43) is obtained from the transpose of Eq. (2.36). Substituting T_{13} and the formal solution for T_{33} (Eq. (2.45)) into the expression for T_{23} , one obtains

$$\begin{aligned} T_{23} &= V_{23} + V_{21}\tilde{G}_1\tilde{V}_{12}\tilde{G}_2V_{23} \\ &\quad + (V_{22} + V_{23}G_3V_{32})G_2T_{23}. \end{aligned} \quad (2.46)$$

Observing that the coefficient in front of G_2T_{23} is simply $\Sigma + K$, one collects all terms proportional to T_{23} and obtains

$$\begin{aligned} T_{23} &= (1 - \Sigma G_2 - K G_2)^{-1}(V_{23} + V_{21}\tilde{G}_1\tilde{V}_{12}\tilde{G}_2V_{23}), \\ &= G_2^{-1}\tilde{G}_2(1 - K\tilde{G}_2)^{-1}(V_{23} + V_{21}\tilde{G}_1\tilde{V}_{12}\tilde{G}_2V_{23}), \\ T_{23} &= G_2^{-1}\tilde{G}_2(\tilde{V}_{23} + t^{(1)}\tilde{G}_2V_{23}). \end{aligned} \quad (2.47)$$

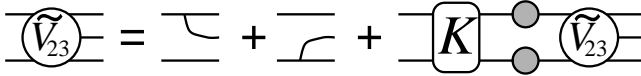


FIG. 6. Schematic diagram for the integral equation in Eq. (2.48) that determines the dressed vertex \tilde{V}_{23} .

The final equality is the desired closed-form expression for T_{23} . It is given in terms of $t^{(1)}$ from Eq. (2.41), the dressed two-body Green function \tilde{G}_2 and the *dressed* vertex,

$$\begin{aligned}\tilde{V}_{23} &= V_{23} + K \tilde{G}_2 \tilde{V}_{23} \\ &= (1 - K \tilde{G}_2)^{-1} V_{23}.\end{aligned}\quad (2.48)$$

A schematic diagram of the dressed vertex \tilde{V}_{23} defined in Eq. (2.48), is shown in Fig. 6. From Eq. (2.47) and Eq. (2.45), the solution to T_{33} is simply

$$T_{33} = V_{32} \tilde{G}_2 \tilde{V}_{23} + V_{32} \tilde{G}_2 t^{(1)} \tilde{G}_2 V_{23}.\quad (2.49)$$

In summary, once the theory has been truncated to include only one-, two- and three-particle states, one can obtain a complete solution for the scattering problem in terms of three integral equations. The closed-form integral equations that one must solve are given in Eqs. (2.34), (2.42), and (2.48). The solution of these three equations can be obtained from the inverse of the operator $1 - K \tilde{G}_2$. In essence, only a single equation must be inverted to solve all three integral equations. That is, once the inverse of the operator $1 - K \tilde{G}_2$ is obtained, the solution to the entire scattering problem is constructed by performing several straightforward integrations.

C. Summary of dynamical restrictions

Having obtained the formal scattering solutions for our relativistic quantum mechanical framework, we give a short summary of the dynamical restrictions placed on the approach. First, the Hilbert space is truncated to include only one-, two- and three-particle states. For some processes, this truncation may not be adequate. For example, processes in which four-particle states are important probably would not be well-described within such a framework. However, it is possible that some of the effects of states with higher particle numbers could be reproduced in a phenomenological manner. For example, if it were essential to include effects of four-pion correlations, one could account for much of the experimental strength by including two body states such as $|\sigma\sigma\rangle$, $|\rho\rho\rangle$ and $|\sigma\rho\rangle$, which would have a significant overlap with the four-pion states.

Next, we have set $V_{33} = 0$ and $V_{31} = V_{13} = 0$. Such interactions may be important to particular channels. For example, an accurate picture of the isoscalar $I = 0$, $J^{PC} = 1^{--}$ channel might require the introduction of

the potential V_{31} to properly account for the direct decay of the ω meson into three pions. Such terms are not believed to be important to the pion scattering application considered in Sec. IV, and so are neglected in this study. However, the inclusion of terms like V_{31} will be incorporated into this framework in future studies.

The final restriction is our assumption that the one- and two-body states do not mix by means of self-energy insertions. (This condition is imposed in the following section.) It is important to note that states may mix through the kernel interaction K , and this type of mixing is already included in our framework. The one- and two-body states employed in the application to $\pi\pi$ scattering considered in Sec. IV can *not* mix by means of the self-energies Σ and Π . Hence, this restriction is irrelevant to the present study. Nonetheless, such mixings are possible in general. In Sec. III C, we will find that although the inclusion of this type of mixing may be straightforward, it does require a reformulation of how mass counter terms are implemented in our framework. The necessary generalization will be discussed elsewhere.

Modulo the restrictions summarized here, the exact solution of the general multi-channel scattering problem is provided by the above closed-system of integral equations.

III. LIPPMANN-SCHWINGER EQUATIONS IN PARTIAL-WAVE BASIS

In the previous section, the formal solution of the Lippmann-Schwinger equation (2.13) was obtained by truncating the Hilbert space to one-, two-, and three-body states, and subject to the restrictions outlined in Sec. II C. The dynamics of these states are given by the coupled set of one-, two- and three-body integral equations Eqs. (2.31), (2.35), (2.36), (2.40), (2.47) and (2.49). In the following, this system of equations is rewritten in the partial-wave basis, and numerical methods necessary to solve these equations are discussed.

A general N -body state is denoted by

$$|\alpha \mathbf{p}_1 \dots \mathbf{p}_N\rangle\quad (3.1)$$

where \mathbf{p}_i is the momentum of the i^{th} particle and α stands for all remaining quantum numbers necessary to uniquely specify the N particle state; that is, the masses $m_{\alpha_1}, m_{\alpha_2}, \dots, m_{\alpha_N}$, total spins $s_{\alpha_1}, s_{\alpha_2}, \dots, s_{\alpha_N}$, spin projections $\lambda_{\alpha_1}, \lambda_{\alpha_2}, \dots, \lambda_{\alpha_N}$, isospins $I_{\alpha_1}, I_{\alpha_2}, \dots, I_{\alpha_N}$, and isospin projections $\kappa_{\alpha_1}, \kappa_{\alpha_2}, \dots, \kappa_{\alpha_N}$. These N -body states are normalized in the canonical manner,

$$\begin{aligned}\langle \beta \mathbf{q}_1 \mathbf{q}_2 \dots \mathbf{q}_N | \alpha \mathbf{p}_1 \mathbf{p}_2 \dots \mathbf{p}_N \rangle &= \\ \delta_{\beta\alpha} \prod_{i=1}^N 2\mathcal{E}(m_{\alpha_i}, \mathbf{p}_i) (2\pi)^3 \delta(\mathbf{q}_i - \mathbf{p}_i),\end{aligned}\quad (3.2)$$

where the free energy of the i^{th} particle is given by

$$\mathcal{E}(m_{\alpha_i}, \mathbf{p}_i) = \sqrt{m_{\alpha_i}^2 + \mathbf{p}_i^2}, \quad (3.3)$$

and the $\delta_{\beta\alpha}$ denotes the product of Kronecker delta functions,

$$\delta_{\beta\alpha} = \prod_{i=1}^N \delta_{m_{\beta_i} m_{\alpha_i}} \delta_{s_{\beta_i} s_{\alpha_i}} \delta_{\lambda_{\beta_i} \lambda_{\alpha_i}} \delta_{I_{\beta_i} I_{\alpha_i}} \delta_{\kappa_{\beta_i} \kappa_{\alpha_i}}. \quad (3.4)$$

The total momentum of the N -body state is given by the sum

$$\mathbf{P} = \sum_{i=1}^N \mathbf{p}_i, \quad (3.5)$$

and the free invariant mass of the N -particle system is given by,

$$\mathcal{M}_{\alpha_1 \dots \alpha_N}(\mathbf{p}_1, \mathbf{p}_2, \dots, \mathbf{p}_N) = \sqrt{\left(\sum_{i=1}^N \mathcal{E}(m_{\alpha_i}, \mathbf{p}_i)\right)^2 - \mathbf{P}^2}. \quad (3.6)$$

Finally, the total free energy is

$$\sum_{i=1}^N \mathcal{E}(m_{\alpha_i}, \mathbf{p}_i) = \mathcal{E}(\mathcal{M}_{\alpha_1 \dots \alpha_N}(\mathbf{p}_1, \mathbf{p}_2, \dots, \mathbf{p}_N), \mathbf{P}). \quad (3.7)$$

In Sections III C and III D, the solutions to the coupled LSEs are obtained using a partial-wave basis involving *relative* momenta rather than the individual particle momenta, \mathbf{p}_i for $i = 1, 2, \dots, N$ introduced above. In the following subsection, we provide a brief review of some of the properties of the N -particle representation of the Poincare group.

A. Relativistic relative momenta

In this section, some important relations for the relativistic relative coordinates are discussed and details of the basic construction of relative coordinates are given. Also, explicit forms of the potential matrix elements are provided in the partial wave basis and in terms of the relative momenta introduced in Sec. II. In the following, the construction of the two-body relative momentum is discussed first. Then, the two-body results are used to construct the three-body relative momenta. Using this approach, it is quite easy to see how the construction of relative momenta can be generalized up to N -body systems.

The relativistic relative momentum of the two-body system is constructed by considering two particles in their center-of-momentum (CM) frame, which is defined by the condition $\mathbf{P} = \mathbf{p}_1 + \mathbf{p}_2 = 0$. In this frame, the momenta of particles 1 and 2 are given by \mathbf{p} and $-\mathbf{p}$, respectively, and \mathbf{p} is defined as the *relative momentum*.

In any other reference frame, the particles will have momenta \mathbf{p}_1 and \mathbf{p}_2 , and the two-body system α_{12} will move with total momentum $\mathbf{P} = \mathbf{p}_1 + \mathbf{p}_2 \neq 0$. An explicit form of the relative momentum \mathbf{p} , given in terms of the momenta \mathbf{p}_1 and \mathbf{p}_2 in any frame, is obtained by performing a boost $\Lambda(0 \leftarrow \mathbf{P})$ on \mathbf{p}_1 from the frame of interest moving with total momentum \mathbf{P} to the CM frame. One finds,

$$\begin{aligned} \mathbf{p} &= \Lambda(0 \leftarrow \mathbf{P}) \mathbf{p}_1, \\ &= \mathbf{p}_1 - \frac{\mathcal{E}(m_{\alpha_1}, \mathbf{p}_1)}{\mathcal{M}_{\alpha_{12}}(\mathbf{p}_1, \mathbf{p}_2)} \mathbf{P} + \frac{\mathbf{P}}{\mathcal{M}_{\alpha_{12}}(\mathbf{p}_1, \mathbf{p}_2)} \\ &\quad \times \frac{\mathbf{p}_1 \cdot \mathbf{P}}{\mathcal{M}_{\alpha_{12}}(\mathbf{p}_1, \mathbf{p}_2) + \mathcal{E}(\mathcal{M}_{\alpha_{12}}(\mathbf{p}_1, \mathbf{p}_2), \mathbf{P})}. \end{aligned} \quad (3.8)$$

The free invariant mass $\mathcal{M}_{\alpha_{12}}$ of a two-body system α_{12} is given in terms of the two momenta \mathbf{p}_1 and \mathbf{p}_2 using Eq. (3.6). The free invariant mass is the same in all frames. Consequently, it depends only on the relative momentum \mathbf{p} and not the total momentum \mathbf{P} ,

$$\begin{aligned} \mathcal{M}_{\alpha_{12}}(\mathbf{p}_1, \mathbf{p}_2) &= \left((\mathcal{E}(m_{\alpha_1}, \mathbf{p}_1) + \mathcal{E}(m_{\alpha_2}, \mathbf{p}_2))^2 \right. \\ &\quad \left. - (\mathbf{p}_1 + \mathbf{p}_2)^2 \right)^{1/2}, \\ &= \mathcal{E}(m_{\alpha_1}, \mathbf{p}) + \mathcal{E}(m_{\alpha_2}, \mathbf{p}), \quad (3.9) \\ &= \mathcal{M}_{\alpha_{12}}(\mathbf{p}). \quad (3.10) \end{aligned}$$

In the following sections, the invariant mass $\mathcal{M}_{\alpha_{12}}(\mathbf{p})$ is almost always written as a function of the relative momentum \mathbf{p} of the two-body system α_{12} , rather than as a function of the individual momenta \mathbf{p}_1 and \mathbf{p}_2 .

Using the total and relative momenta \mathbf{P} and \mathbf{p} , respectively, the two-body system α_{12} is described by the ket $|\alpha \mathbf{P} \mathbf{p}\rangle$. In Eq. (3.2), the canonical normalization of an N -body state was given in terms of the individual particle momenta. It is convenient to rewrite the normalization condition in terms of these momenta. The normalization of two-particle states becomes

$$\begin{aligned} \langle \beta \mathbf{Q} \mathbf{q} | \alpha \mathbf{P} \mathbf{p} \rangle &= (2\pi)^3 \delta(\mathbf{Q} - \mathbf{P}) \delta_{\beta\alpha} 2\mathcal{E}(\mathcal{M}_{\alpha_{12}}(\mathbf{p}), \mathbf{P}) \\ &\quad \times \rho_{\alpha_{12}}^{-1}(\mathbf{p}) (2\pi)^3 \delta(\mathbf{q} - \mathbf{p}), \end{aligned} \quad (3.11)$$

where the two-body Jacobian, $\rho_{\alpha_{12}}$ is given by

$$\rho_{\alpha_{12}}(\mathbf{p}) = \frac{\mathcal{M}_{\alpha_{12}}(\mathbf{p})}{2\mathcal{E}(m_{\alpha_1}, \mathbf{p})\mathcal{E}(m_{\alpha_2}, \mathbf{p})}, \quad (3.12)$$

Proceeding in a similar manner, one may now construct suitable definitions for the relative and total momenta for a three-body system α_{123} . A unique description of a three-body system α_{123} requires three momenta \mathbf{p}_1 , \mathbf{p}_2 , and \mathbf{p}_3 . In terms of relative coordinates, the set of three momenta consists of one total momentum $\mathbf{P} = \mathbf{p}_1 + \mathbf{p}_2 + \mathbf{p}_3$, and *two* relative momenta.

Consider the three-body system α_{123} which can be described in terms of the individual particle momenta \mathbf{p}_1 ,

\mathbf{p}_2 , and \mathbf{p}_3 . The state associated with this system of particles is given by the ket $|\alpha_{\mathbf{p}_1\mathbf{p}_2\mathbf{p}_3}\rangle$. One defines a two-body *subsystem* α_{23} consisting of the second and third particles and writes the relative momentum between them as \mathbf{p}_{23} . In an analogy to the two-body case discussed earlier, the relative momentum \mathbf{p}_{23} is defined as the momentum of particle 2 in the CM frame of the α_{23} subsystem where $\mathbf{p}_2 + \mathbf{p}_3 = 0$; in the CM frame of the subsystem α_{23} , the relative momentum $\mathbf{p}_{23} = \mathbf{p}_2 = -\mathbf{p}_3$.

In a frame in which the two-body subsystem α_{23} moves with a total momentum $\mathbf{P}_{23} = \mathbf{p}_2 + \mathbf{p}_3$, the relative momentum \mathbf{p}_{23} is obtained using a boost similar to that of Eq. (3.8),

$$\begin{aligned} \mathbf{p}_{23} &= \mathbf{p}_2 - \frac{\mathcal{E}(m_{\alpha_2}, \mathbf{p}_2)}{\mathcal{M}_{\alpha_{23}}(\mathbf{p}_2, \mathbf{p}_3)} \mathbf{P}_{23} + \frac{\mathbf{P}_{23}}{\mathcal{M}_{\alpha_{23}}(\mathbf{p}_2, \mathbf{p}_3)} \\ &\times \frac{\mathbf{p}_2 \cdot \mathbf{P}_{23}}{\mathcal{M}_{\alpha_{23}}(\mathbf{p}_2, \mathbf{p}_3) + \mathcal{E}(\mathcal{M}_{\alpha_{23}}(\mathbf{p}_2, \mathbf{p}_3), \mathbf{P}_{23})}. \end{aligned} \quad (3.13)$$

The second relative momentum is defined relative to particle 1 and the two-body subsystem α_{23} ; it is referred to as \mathbf{p} . In the CM frame of the three-body system α_{123} $\mathbf{P} = \mathbf{p}_1 + \mathbf{p}_2 + \mathbf{p}_3 = 0$, and the relative momentum \mathbf{p} is defined as the momentum of the two-body subsystem α_{23} . In the CM frame of the three-body system α_{123} , the two-body subsystem α_{23} moves with a momentum $\mathbf{p} = \mathbf{P}_{23}$ and particle 1 moves with momentum $\mathbf{p}_1 = -\mathbf{p}$. The relative momenta \mathbf{p} and \mathbf{p}_{23} and total momentum \mathbf{P} for the three-body system α_{123} are shown schematically in Fig. 7.

In following sections, numerical calculations will be carried out in the CM frame where the total momentum $\mathbf{P} = 0$. In this frame the three-body state is given by the ket $|\alpha_{\mathbf{P}\mathbf{p}\mathbf{p}_{23}}\rangle$, where the explicit relation between the relative momenta and the individual particle momenta \mathbf{p}_1 , \mathbf{p}_2 , and \mathbf{p}_3 are

$$\begin{aligned} \mathbf{P} &= \mathbf{p}_1 + \mathbf{p}_2 + \mathbf{p}_3 = 0, \\ \mathbf{p} &= -\mathbf{p}_1, \end{aligned} \quad (3.14)$$

and the relative momentum \mathbf{p}_{23} is

$$\begin{aligned} \mathbf{p}_{23} &= \mathbf{p}_2 - \frac{\mathcal{E}(m_{\alpha_2}, \mathbf{p}_2)}{\mathcal{M}_{\alpha_{23}}(\mathbf{p}_2, \mathbf{p}_3)} \mathbf{P} + \frac{\mathbf{p}}{\mathcal{M}_{\alpha_{23}}(\mathbf{p}_2, \mathbf{p}_3)} \\ &\times \frac{\mathbf{p}_2 \cdot \mathbf{p}}{\mathcal{M}_{\alpha_{23}}(\mathbf{p}_2, \mathbf{p}_3) + \mathcal{E}(\mathcal{M}_{\alpha_{23}}(\mathbf{p}_2, \mathbf{p}_3), \mathbf{p})}. \end{aligned} \quad (3.15)$$

The generalization to N -body states is obvious.

The normalization of the three-body state $|\alpha_{\mathbf{P}\mathbf{p}\mathbf{p}_{23}}\rangle$ can now be given in terms of the relative momenta \mathbf{p}_{23} and \mathbf{p} , and the total momentum \mathbf{P} by

$$\begin{aligned} \langle \beta \mathbf{Q} \mathbf{q} \mathbf{q} \mathbf{q}_{23} | \alpha_{\mathbf{P}\mathbf{p}\mathbf{p}_{23}} \rangle &= \delta_{\beta\alpha} 2\mathcal{E}(\mathcal{M}_{\alpha_{123}}(\mathbf{p}, \mathbf{p}_{23}), \mathbf{P}) (2\pi)^9 \\ &\times \delta(\mathbf{Q} - \mathbf{P}) \delta(\mathbf{q} - \mathbf{p}) \delta(\mathbf{q}_{23} - \mathbf{p}_{23}) \\ &\times \rho_{\alpha_{123}}^{-1}(\mathbf{p}, \mathbf{p}_{23}) \rho_{\alpha_{23}}^{-1}(\mathbf{p}_{23}), \end{aligned} \quad (3.16)$$

where the three-body Jacobian and the three-body free invariant mass are given by,

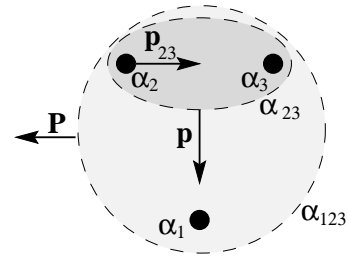


FIG. 7. Schematic diagram showing the definitions of three-body relative momenta. The three-body system α_{123} moves with total momentum \mathbf{P} , the relative momentum between the two-body subsystem α_{23} and particle 1 is \mathbf{p} , and the relative momentum between particles 2 and 3 is \mathbf{p}_{23} . The relative momenta \mathbf{p} and \mathbf{p}_{23} are defined in the CM frame of the three-body system α_{123} and the two-body system α_{23} , respectively.

$$\rho_{\alpha_{123}}(\mathbf{p}, \mathbf{p}_{23}) = \frac{\mathcal{M}_{\alpha_{123}}(\mathbf{p}, \mathbf{p}_{23})}{2\mathcal{E}(\mathcal{M}_{\alpha_{23}}(\mathbf{p}_{23}), \mathbf{p})\mathcal{E}(m_{\alpha_1}, -\mathbf{p})}, \quad (3.17)$$

$$\mathcal{M}_{\alpha_{123}}(\mathbf{p}, \mathbf{p}_{23}) = \mathcal{E}(m_{\alpha_1}, -\mathbf{p}) + \mathcal{E}(\mathcal{M}_{\alpha_{23}}(\mathbf{p}_{23}), \mathbf{p}), \quad (3.18)$$

respectively. The similarity between the two- and three-body Jacobians in Eqs. (3.12) and (3.17) is clear. In the notation employed herein, the two- and three-body Jacobians are distinguished from each other solely by the number of arguments (and subscripts) each takes. Since these Jacobians depend only on relative momenta, the two-body Jacobian $\rho_{\alpha_{12}}(\mathbf{p})$ in Eq. (3.12) depends on the single momentum \mathbf{p} , while the three-body Jacobian $\rho_{\alpha_{123}}(\mathbf{p}, \mathbf{p}_{23})$ in Eq. (3.17) depends on the two relative momenta \mathbf{p}_{23} and \mathbf{p} .

In Eq. (3.16), one observes that the three-body normalization condition contains both two- and three-body Jacobians. The two-body Jacobian $\rho_{\alpha_{23}}(\mathbf{p}_{23})$ is associated with the internal dynamics of the two-body subsystem α_{23} , while the three-body Jacobian $\rho_{\alpha_{123}}(\mathbf{p}, \mathbf{p}_{23})$ is associated with the relative motion between particle 1 and the two-body subsystem α_{23} .

B. Potential matrix elements

In Sec. II B, forms for the LSEs were derived and their formal solutions were given in terms of matrix elements of the potential operator V of Eq. (2.19). In the following, solutions for the LSEs will be given explicitly in terms of the matrix elements of the potential V . These matrix elements are considered to be the fundamental elements which are defined by an underlying dynamical model. These potential matrix elements are then used to determine all other quantities, such as Green functions and scattering amplitudes.

The potential matrix element V_{21} is the amplitude that describes the coupling of a one-body state to a two-body state. The general form of this matrix element is given by

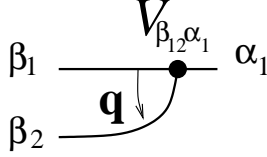


FIG. 8. Diagram depicting the particle and momentum labels of the potential matrix element V_{21} which connects one-body and two-body states, from Eq. (3.22).

$$\langle \beta \mathbf{Q} \mathbf{q} | V_{21} | \alpha \mathbf{P} \rangle = (2\pi)^3 \delta(\mathbf{Q} - \mathbf{P}) \langle \beta_{12} \mathbf{q} | V_{21} | \alpha_1 \rangle_{\mathbf{P}}. \quad (3.19)$$

In a general frame the potential matrix elements in Eq. (3.19) can be complicated if the particles involved have spin. The procedure to include their spin couplings is to boost each of the particles to the CM frame, and couple them together in the usual manner to obtain the total angular momentum J . The spin-coupled two-body system is then boosted back to the original frame where $\mathbf{P} \neq 0$. As observed in Eq. (2.5) of Sec. II, this procedure results in non-trivial rotations of the particle spins which require Wigner rotation matrices $D_{\lambda, \lambda'}^s(\mathbf{P}, \mathbf{p})$. The general result for the matrix element of V_{21} is

$$\langle \beta_{12} \mathbf{q} | V_{21} | \alpha_1 \rangle_{\mathbf{P}} = \sum D_{\lambda_{\beta_1} \lambda'_{\beta_1}}^{s_{\beta_1}}(\mathbf{P}, \mathbf{q}) D_{\lambda_{\beta_2} \lambda'_{\beta_2}}^{s_{\beta_2}}(\mathbf{P}, -\mathbf{q}) \times \langle \beta_{12} \mathbf{q} | V_{21} | \alpha_1 \rangle \quad (3.20)$$

where the sum is over spin projections λ'_{β_1} and λ'_{β_2} . In the CM frame, the reduced matrix element is given by

$$\langle \beta_{12} \mathbf{q} | V_{21} | \alpha_1 \rangle = \sum Y_{L_{\beta} M_{L_{\beta}}}^*(\hat{\mathbf{q}}) \langle L_{\beta} M_{L_{\beta}} S_{\beta} M_{S_{\beta}} | s_{\alpha_1} \lambda_{\alpha_1} \rangle \times \langle s_{\beta_1} \lambda'_{\beta_1} s_{\beta_2} \lambda'_{\beta_2} | S_{\beta} M_{S_{\beta}} \rangle \times \langle I_{\beta_1} \kappa_{\beta_1} I_{\beta_2} \kappa_{\beta_2} | I_{\alpha_1} \kappa_{\alpha_1} \rangle V_{\beta_{12}\alpha_1}(q), \quad (3.21)$$

where the sum is over the orbital angular momentum L_{β} , its projection $M_{L_{\beta}}$, total spin S_{β} and its projection $M_{S_{\beta}}$. The vertex function $V_{\beta_{12}\alpha_1}(q)$ appearing in Eq. (3.21) is defined by

$$V_{\beta_{12}\alpha_1}(q) = \langle q m_{\beta_1} m_{\beta_2} S_{\beta} L_{\beta} s_{\beta_1} s_{\beta_2} I_{\beta_1} I_{\beta_2} | V_{21} | m_{\alpha_1} s_{\alpha_1} I_{\alpha_1} \rangle, \quad (3.22)$$

and is depicted in Fig. 8.

For the particular application to $\pi\pi$ scattering considered in Sec. IV, the two-body states contain only spinless particles (either pions or kaons) and consequently the amplitude in Eq. (3.20) simplifies considerably. For spinless two-body states $|\beta \mathbf{Q} \mathbf{q}\rangle$, Eq. (3.20) reduces to

$$\langle \beta_{12} \mathbf{q} | V_{21} | \alpha_1 \rangle_{\mathbf{P}} = Y_{s_{\alpha_1} \lambda_{\alpha_1}}^*(\hat{\mathbf{q}}) \langle I_{\beta_1} \kappa_{\beta_1} I_{\beta_2} \kappa_{\beta_2} | I_{\alpha_1} \kappa_{\alpha_1} \rangle \times V_{\beta_{12}\alpha_1}(q). \quad (3.23)$$

Another simplification encountered in the phenomenological model employed in Sec. IV, is that potentials connecting three-body states to two-body states are assumed

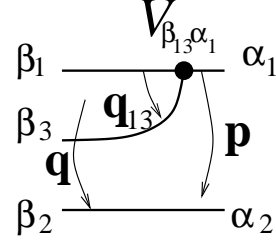


FIG. 9. Diagram depicting the particle labels and momenta for the potential $V_{32}^{(1)}$ that connects two- and three-body states, from Eq. (3.26).

to arise when one of the particles emits or absorbs a particle while the other acts like a spectator. Such potentials can be expressed as the sum of two terms,

$$V_{32} = V_{32}^{(1)} + V_{32}^{(2)}, \quad (3.24)$$

where $V_{32}^{(i)}$ denotes the transition from a two-body to three-body state for which the i^{th} particle in the two-body state emits particle 3 of the three-body state. The matrix element of $V_{32}^{(1)}$ is

$$\langle \beta \mathbf{Q} \mathbf{q} \mathbf{q}_{13} | V_{32}^{(1)} | \alpha \mathbf{P} \mathbf{p} \rangle = (2\pi)^3 \delta(\mathbf{Q} - \mathbf{P}) \times \langle \beta_{123} \mathbf{q} \mathbf{q}_{13} | V_{32}^{(1)} | \alpha_{12} \mathbf{p} \rangle_{\mathbf{P}}. \quad (3.25)$$

In the CM frame $\mathbf{P} = 0$, the above matrix element is of the form

$$\langle \beta_{123} \mathbf{q} \mathbf{q}_{13} | V_{32}^{(1)} | \alpha_{12} \mathbf{p} \rangle_{\mathbf{P}=0} = (2\pi)^3 \delta(\mathbf{q} - \mathbf{p}) \times 2\mathcal{E}(m_{\beta_2}, -\mathbf{p}) \delta_{\beta_2\alpha_2} \times \langle \beta_{13} \mathbf{q}_{13} | V_{21} | \alpha_1 \rangle_{\mathbf{p}}, \quad (3.26)$$

where $\langle \beta_{13} \mathbf{q}_{13} | V_{21} | \alpha_1 \rangle_{\mathbf{p}}$ is the amplitude for α_1 to couple to β_1 and β_3 given by Eq. (3.20), and particle α_2 is a spectator. The form of the matrix element for $V_{32}^{(1)}$ and the relevant kinematics are depicted in Fig. 9. One important aspect of Eq. (3.26) is that as long as *any* of the particles in the three-body state has non-zero spin, one must use the general form for V_{21} from Eq. (3.20), rather than the simpler form given in Eq. (3.23).

Finally, the potential matrix element V_{11} connects one-body states to other one-body states. It is given by

$$\langle \beta \mathbf{Q} | V_{11} | \alpha \mathbf{P} \rangle = (2\pi)^3 \delta(\mathbf{Q} - \mathbf{P}) 2\sqrt{m_{\beta_1} m_{\alpha_1}} \delta \Pi_{\beta\alpha}(\mathbf{P}). \quad (3.27)$$

This matrix element is referred to as the one-body self-energy counter term. It will appear in the one-body self-energy, where it adds to the one-body mass, however $\delta \Pi_{\beta\alpha}(\mathbf{P})$ may have non-trivial off-diagonal elements in the channel indices α and β . Such off-diagonal elements would result in a mixing between one-body states, but such a possibility will not be addressed in this paper. The value of $\delta \Pi_{\beta\alpha}(\mathbf{P})$ will be determined by requiring the one-body propagator \tilde{G}_1 to have poles for energies

equal to the physical one-body masses. Conservation of angular momentum and isospin requires that $\delta\Pi_{\beta\alpha}(\mathbf{P})$ is diagonal in spins and isospins and does not depend on spin or isospin projections.

In this section, the matrix elements of the potential V from Eq. (2.19) have been provided in terms of reduced matrix elements, such as $\delta\Pi_{\beta\alpha}$ and $V_{\beta_{12}\alpha_1}(q)$. These reduced matrix elements are real-valued functions and the particular form of these functions is dictated by the dynamical model under consideration. In Sec. IV, we describe a simple model of these elements, which provides an excellent description of $\pi\pi$ scattering from threshold to 1400 MeV. In the following subsections, explicit forms for all other elements of the framework are given in terms of the above reduced matrix elements.

C. Self-energies

Explicit forms for the matrix elements obtained in the previous section can now be inserted into the expressions for the one-body self-energy $\Pi_{\beta\alpha}$ given by Eq. (2.33), and for the two-body self-energy $\Sigma_{\beta\alpha}$ to be given by Eq. (3.35). In this section, we provide explicit forms of the one- and two-body self-energies, and we review the techniques necessary to calculate them.

From Eq. (2.33), it is clear that the evaluation of the one-body self-energy $\Pi_{\beta\alpha}$ requires knowledge of the dressed two-body propagator \tilde{G}_2 , defined in Eq. (2.29), and the dressed vertex \tilde{V}_{21} , defined in Eq. (2.34). While the latter depends on the two-body scattering kernel K , both depend on the two-body self-energy $\Sigma_{\beta\alpha}$. For this reason, it is convenient to discuss the solution of the two-body self-energy $\Sigma_{\beta\alpha}$ prior to discussing the one-body self-energy $\Pi_{\beta\alpha}$.

1. Two-body self-energy

An explicit form for the two-body free Green function with driving energy E is obtained by evaluating the operator

$$G_2 = (E - H + i\epsilon)^{-1} \quad (3.28)$$

between two two-body eigenstates of the free Hamiltonian H ,

$$\langle\beta\mathbf{Q}\mathbf{q}|G_2|\alpha\mathbf{P}\mathbf{p}\rangle = (2\pi)^3\delta(\mathbf{Q}-\mathbf{P})\langle\beta_{12}\mathbf{q}|G_2|\alpha_{12}\mathbf{p}\rangle_{\mathbf{P}}, \quad (3.29)$$

and in the CM frame $\mathbf{P} = 0$,

$$\langle\beta_{12}\mathbf{q}|G_2|\alpha_{12}\mathbf{p}\rangle_{\mathbf{P}=0} = 2\mathcal{M}_{\alpha_{12}}(p)(2\pi)^3\delta(\mathbf{q}-\mathbf{p}) \times \frac{1}{p^2\rho_{\alpha_{12}}(p)}G_{\beta\alpha}(p, E). \quad (3.30)$$

Here, $\mathcal{M}_{\alpha_{12}}(p)$ is the free invariant mass of the two-body state $|\alpha\mathbf{P}\mathbf{p}\rangle$, \mathbf{p} , \mathbf{q} are the relative momentum of the two-body systems α and β , respectively, and $\rho_{\alpha_{12}}(p)$ is the two-body Jacobian from Eq. (3.12). From Eq. (3.30), the free Green function in the CM frame is then given by

$$G_{\beta\alpha}(p, E) = \frac{\delta_{\beta\alpha}}{E - \mathcal{M}_{\alpha_{12}}(p) + i\epsilon}. \quad (3.31)$$

To obtain the dressed two-body Green function, one must first derive the reduced matrix element for the two-body self-energy $\Sigma_{\beta\alpha}(p, E)$. This is done by evaluating the matrix element of operator in Eq. (2.26) between two-body eigenstates of \mathcal{M} and keeping only terms that are proportional to $\delta(\mathbf{q}-\mathbf{p})$. These are identified with the two-body self-energy Σ and are given by,

$$\langle\beta_{12}\mathbf{q}|\Sigma|\alpha_{12}\mathbf{p}\rangle_{\mathbf{P}=0} = 2\sqrt{\mathcal{M}_{\beta_{12}}(q)\mathcal{M}_{\alpha_{12}}(p)} \times (2\pi)^3\delta(\mathbf{q}-\mathbf{p}) \frac{\Sigma_{\beta\alpha}(p, E)}{pq\sqrt{\rho_{\beta_{12}}(q)\rho_{\alpha_{12}}(p)}}. \quad (3.32)$$

It is important to observe, that just like the matrix element for the two-body free Green function, the two-body self-energy is symmetric in the channel indices α and β . However, unlike the free Green function, the two-body self-energy $\Sigma_{\beta\alpha}(p, E)$ is *not* necessarily diagonal in these indices; self-interactions may lead to a mixing of the different channels. It follows that the dressed Green function of Eq. (2.28) may also be non-diagonal in general.

The reduced matrix elements for the *dressed* Green function \tilde{G}_2 defined by Eq. (2.28) are

$$\langle\beta_{12}\mathbf{q}|\tilde{G}_2|\alpha_{12}\mathbf{p}\rangle_{\mathbf{P}=0} = 2\sqrt{\mathcal{M}_{\beta_{12}}(q)\mathcal{M}_{\alpha_{12}}(p)} \times (2\pi)^3\delta(\mathbf{q}-\mathbf{p}) \frac{\tilde{G}_{\beta\alpha}(p, E)}{pq\sqrt{\rho_{\beta_{12}}(q)\rho_{\alpha_{12}}(p)}}, \quad (3.33)$$

where

$$\tilde{G}_{\beta\alpha}(p, E) = \left(\delta_{\alpha\beta}(E - \mathcal{M}_{\alpha_{12}}(p) + i\epsilon) - \Sigma_{\alpha\beta}(p, E) \right)^{-1}. \quad (3.34)$$

One can collect the terms from Eq. (2.26) contributing to the two-body self-energy $\Sigma_{\beta\alpha}$, and organize them into the following sum,

$$\Sigma = \delta\Sigma + V_{23}^{(1)}G_3V_{32}^{(1)} + V_{23}^{(2)}G_3V_{32}^{(2)}. \quad (3.35)$$

Here, the superscript (i) refers to the diagram in which the i^{th} particle in the two-body state emits and subsequently re-absorbs the particle γ_3 . The term $\delta\Sigma$ is identified with the part of the potential V_{22} that is proportional to a Dirac δ -function in the relative two-body momentum, as discussed in Sec. II B. (All other terms that appear in Eq. (2.26) but which do not appear in Σ in Eq. (3.35), are part of the two-body kernel K .)

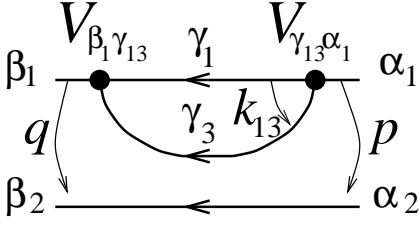


FIG. 10. Diagram depicting one of the contributions to the two-body self-energy $\Sigma_{\beta\alpha}^{(1)}(p, E)$ given in Eq. (3.36). Shown here, particle α_1 decays into particles γ_1 and γ_3 , and these subsequently recombine to form particle β_1 . The relative momentum between the intermediate particles γ_1 and γ_3 is k_{13} , the relative momentum of the incoming state $|\alpha\mathbf{p}_1\mathbf{p}_2\rangle$ is p , and relative momentum of the outgoing state $|\beta\mathbf{q}_1\mathbf{q}_2\rangle$ is q . Solid circles denote matrix elements of the potentials from Eq. (2.19), $V_{\beta_1\gamma_{13}}$ and $V_{\gamma_{13}\alpha_1}$, evaluated between two- and three-body states.

Upon inserting a complete set of three-body states into Eq. (3.35) and evaluating the resulting expressions in the overall CM frame with $\mathbf{P} = 0$, one obtains

$$\begin{aligned} \Sigma_{\beta\alpha}^{(1)}(p, E) &= \sum_{\gamma_{13}} \int_0^\infty dk_{13} \frac{a_{\gamma_{13}}(k_{13}, p)}{2\sqrt{\mathcal{E}(m_{\beta_1}, p)}\mathcal{E}(m_{\alpha_1}, p)} \\ &\times V_{\beta_1\gamma_{13}}(k_{13}) G_\gamma(p, k_{13}, E) V_{\gamma_{13}\alpha_1}(k_{13}), \end{aligned} \quad (3.36)$$

and

$$\begin{aligned} \Sigma_{\beta\alpha}^{(2)}(p, E) &= \sum_{\gamma_{23}} \int_0^\infty dk_{23} \frac{a_{\gamma_{23}}(k_{23}, -p)}{2\sqrt{\mathcal{E}(m_{\beta_2}, -p)}\mathcal{E}(m_{\alpha_2}, -p)} \\ &\times V_{\beta_2\gamma_{23}}(k_{23}) G_\gamma(p, k_{23}, E) V_{\gamma_{23}\alpha_2}(k_{23}), \end{aligned} \quad (3.37)$$

where $\Sigma^{(i)} = V_{23}^{(i)} G_3 V_{32}^{(i)}$. The integrations are over the relative momenta between two of the particles in the three-body intermediate state, J is the total angular momentum of the system, the sum is over all three-body states γ , and we have introduced the three-body Green function,

$$G_\gamma(p, k_{13}, E) = \frac{1}{E - \mathcal{M}_{\gamma_{123}}(p, k_{13}) + i\epsilon}. \quad (3.38)$$

For brevity the commonly occurring two-body phase space factor,

$$a_{\gamma_{13}}(k_{13}, p) = \frac{k_{13}^2}{(2\pi)^3} \frac{\rho_{\gamma_{13}}(k_{13})}{2\mathcal{E}(\mathcal{M}_{\gamma_{13}}(k_{13}), p)}, \quad (3.39)$$

has been introduced. The expression in Eq. (3.36) for the two-body self-energy $\Sigma_{\beta\alpha}^{(1)}(p, E)$ is depicted in Fig. 10. In the CM frame, the two-body self-energy $\Sigma_{\beta\alpha}(p, E)$ is then the sum of these two terms and the two-body mass counter term $\delta\Sigma_{\beta\alpha}(p)$,

$$\Sigma_{\beta\alpha}(p, E) = \delta\Sigma_{\beta\alpha}(p) + \Sigma_{\beta\alpha}^{(1)}(p, E) + \Sigma_{\beta\alpha}^{(2)}(p, E). \quad (3.40)$$

Evaluation of the two-body self-energy $\Sigma_\alpha(p, E)$ requires calculating the imaginary part and a principal part of the integrals in Eqs. (3.36) and (3.37). For energies E above a three-body threshold, these integrals encounter poles in the three-body Green function. For example, in Eq. (3.36), the three-body Green function, defined in Eq. (3.38), exhibits a pole at the relative momentum $k_{13} = k_{0\gamma}$, where the quantity $k_{0\gamma}$ satisfies the relation

$$E - \mathcal{M}_{\gamma_{123}}(p, k_{0\gamma}) = 0. \quad (3.41)$$

The location of the three-body pole of the k_{13} -integral in Eq. (3.36) is obtained by inverting the relation in Eq. (3.41). One obtains,

$$k_{0\gamma}^2(p, E) = \frac{A^2 - m_{\gamma_1}^2 m_{\gamma_3}^2}{2A + m_{\gamma_1}^2 + m_{\gamma_3}^2}, \quad (3.42)$$

where

$$A(p, E) = \frac{1}{2}([E - \mathcal{E}(m_{\gamma_2}, p)]^2 - p^2 - m_{\gamma_1}^2 - m_{\gamma_3}^2), \quad (3.43)$$

with the additional constraints that

$$\begin{aligned} k_{0\gamma}^2(p, E) &\geq A(p, E), \\ p^2 &\leq E^2 - m_{\gamma_2}^2. \end{aligned} \quad (3.44)$$

A similar expression can be obtained for the integral in Eq. (3.37) as well.

The integrations necessary to determine the self-energies from Eqs. (3.36) and (3.37) involve both real and imaginary parts. They are calculated separately using the following identity for the three-body Green function,

$$\begin{aligned} G_\gamma(p, k, E) &= -i\pi\delta[E - \mathcal{M}_{\gamma_{123}}(p, k)] \\ &+ \frac{\mathcal{P}}{E - \mathcal{M}_{\gamma_{123}}(p, k)}. \end{aligned} \quad (3.45)$$

If the energy is below the three-body threshold energy $\mathcal{M}_{\gamma_{123}}(p, k)$, the delta-function will always vanish, ensuring that the three-body Green function acquires an imaginary part only for energies above the three-body threshold. The appearance of the Dirac delta function provides us with an analytic expression for the imaginary part of the two-body self-energy. The real part is calculated directly using an adaptive integration routine. The numerical routine employed is stable only when the adiabatic switching scale ϵ is non-zero. The numerical results depend very weakly on the value of the parameter ϵ , provided that it is sufficiently small. This issue is explored in detail in Sec. III E.

Having evaluated the contribution to the two-body self-energy from the integrals in Eqs. (3.36) and (3.37), all that remains to completely determine the two-body self-energy $\Sigma_{\beta\alpha}(p, E)$ is to determine the two-body mass counter term $\delta\Sigma_{\beta\alpha}(p)$. The counter term $\delta\Sigma_{\beta\alpha}(p)$ can depend only on the relative momentum p of the two-body system. Recall that it arises directly as a matrix element

of the potential V_{22} . Hence, it is necessarily a real-valued function, independent of the driving energy E and total momentum \mathbf{P} . Both of these features are necessary to ensure the unitarity of the theory and covariance of obtained observables.

As discussed in Secs. III C 1 and III C 2, it is assumed that the two-body self-energy $\Sigma_{\beta\alpha}(p, E)$ does not mix different channels; that is, the self energy is of the form,

$$\Sigma_{\beta\alpha}(p, E) \rightarrow \delta_{\beta\alpha}\Sigma_{\alpha}(p, E). \quad (3.46)$$

Hence, the counter term is simply chosen to be

$$\delta\Sigma_{\alpha}(p) = -\left(\Sigma_{\alpha}^{(1)}(p, E) + \Sigma_{\alpha}^{(2)}(p, E)\right)_{E=\mathcal{M}_{\alpha_{12}}(p)}. \quad (3.47)$$

This is necessary and sufficient to ensure unitarity and that the stable two-body system α_{12} is observed asymptotically with the invariant mass $\mathcal{M}_{\alpha_{12}}(p)$.

2. One-body self-energy

The formal solution for the one-body self-energy is given in Eq. (2.33). The matrix elements of Π are

$$\begin{aligned} \langle\beta\mathbf{Q}|\Pi|\alpha\mathbf{P}\rangle &= (2\pi)^3\delta(\mathbf{Q}-\mathbf{P})2\sqrt{\mathcal{E}(m_{\beta_1}, \mathbf{Q})\mathcal{E}(m_{\alpha}, \mathbf{P})} \\ &\times \Pi_{\beta\alpha}(\mathbf{P}, E). \end{aligned} \quad (3.48)$$

The self-energy only mixes one-body states of same spin s , spin projection λ , isospin I , and isospin projection κ . As discussed in Sec. II C, the present framework is further restricted to include only one- and two-body self-energies that do not mix different states. With this restriction, one obtains

$$\Pi_{\beta\alpha}(\mathbf{P}, E) = \delta_{\beta\alpha}\Pi_{\alpha}(\mathbf{P}, E). \quad (3.49)$$

To solve for the self-energy, one inserts a complete set of two-body states into the symbolic expression for the one-body self-energy $\Pi_{\alpha}(\mathbf{P}, E)$, which first appeared in Eq. (2.33),

$$\Pi = V_{11} + V_{12}\tilde{G}_2\tilde{V}_{21}. \quad (3.50)$$

Upon using the explicit expressions given by Eqs. (3.23) and (3.33), one obtains an expression for the one-body self-energy in the CM frame with $\mathbf{P} = 0$,

$$\begin{aligned} \Pi_{\alpha}(E) &= \delta\Pi_{\alpha} + \frac{1}{2m_{\alpha_1}}\sum_{\gamma_{12}}\int_0^{\infty}dk a_{\gamma_{12}}(k, 0) \\ &\times V_{\alpha_1\gamma_{12}}(k)\tilde{G}_{\gamma}(k, E)\tilde{V}_{\gamma_{12}\alpha_1}(k, E). \end{aligned} \quad (3.51)$$

In Eq. (3.51), m_{α_1} is the mass of the one-body state $|\alpha\mathbf{P}\rangle$, $V_{\alpha_1\gamma_{12}}(k)$ is the vertex function of the potential V_{12} from Eq. (3.22), $\tilde{V}_{\gamma_{12}\alpha_1}(k, E)$ is the vertex function for the dressed vertex \tilde{V}_{21} , $\tilde{G}_{\gamma}(k, E)$ is the dressed two-body

Green function, and $a_{\gamma_{12}}(k, 0)$ is a factor associated with the phase space of the two-body system γ_{12} . This phase space factor was first introduced in Eq. (3.39). However, it is now evaluated in the CM frame of γ_{12} , and is given by

$$a_{\gamma_{12}}(k, 0) = \frac{k^2}{(2\pi)^3}\frac{\rho_{\gamma_{12}}(k)}{2\mathcal{M}_{\gamma_{12}}(k)}, \quad (3.52)$$

The sum in Eq. (3.51) is taken over all two-body states and their internal quantum numbers, such as spin and isospin.

The two-body self-energy $\Sigma_{\alpha}(p, E)$, originally defined in Eq. (2.26), is given in terms of the elementary bare vertices V_{23} and V_{32} and the free three-body Green function G_3 . In order to evaluate the integral in Eq. (3.51) and obtain the one-body self-energy $\Pi_{\alpha}(E)$, we need to determine the two-body self-energy from Eq. (3.40) with Eqs. (3.36), (3.37), and (3.47), and then the dressed two-body Green function $\tilde{G}_{\gamma}(p, E)$ from Eq. (2.28), and in addition we need the dressed vertex \tilde{V}_{21} . Direct determination of the dressed vertex requires solving an integral equation, which is the subject of Sec. III D. For the present, let us discuss the numerical details necessary to evaluate Eq. (3.51) once the dressed vertices and two-body Green function have been obtained.

The one-body self-energy $\Pi_{\alpha}(E)$ is calculated in the overall CM frame using the method of Gauss quadrature. Of course, the dressed vertex and dressed two-body propagator have also been solved for these values of the relative momentum k . For this reason, it is important to employ a single set of quadrature mesh points for all quantities calculated in this study. Otherwise, interpolation is necessary.

Evaluation of the integral in Eq. (3.51) requires a determination of both the principal part and the imaginary part. The imaginary part arises from the pole in the dressed two-body Green function,

$$\begin{aligned} \tilde{G}_{\gamma}(k, E) &= \frac{1}{E - \mathcal{M}_{\gamma_{12}}(k) - \Sigma_{\gamma}(k, E) + i\epsilon}, \\ &= -i\pi\delta[E - \mathcal{M}_{\gamma_{12}}(k) - \Sigma_{\gamma}(k, E)] \\ &\quad + \frac{\mathcal{P}}{E - \mathcal{M}_{\gamma_{12}}(k) - \Sigma_{\gamma}(k, E)}. \end{aligned} \quad (3.53)$$

The Dirac delta function ensures that the two-body Green function acquires an imaginary part only when the energy E is above the two-body threshold energy. Recall that the choice of mass counter terms, discussed in Sec. III C 1, ensures that the real part of the two-particle self-energy $\text{Re}(\Sigma_{\gamma}(k_{0\gamma}, E)) = 0$, where $k_{0\gamma}$ satisfies the relation $\mathcal{M}_{\gamma_{12}}(k_{0\gamma}) = E$. The Dirac δ -function can be rewritten as a δ -function in the relative momentum k ,

$$\delta[E - \mathcal{M}_{\gamma_{12}}(k) - \Sigma_{\gamma}(k, E)] = \frac{z_{\gamma}}{2k_{0\gamma}\rho_{\gamma_{12}}(k_{0\gamma})}\delta(k_{0\gamma} - k), \quad (3.54)$$

with

$$z_\gamma = \left(1 + \frac{1}{2k_{0\gamma}\rho_{\gamma 12}(k_{0\gamma})} \frac{d}{dk^2} \Sigma_\gamma(k_{0\gamma}, E) \right)^{-1}. \quad (3.55)$$

Herein, z_γ is referred to as the wavefunction renormalization. It is finite. The term arises from the dressing of the two-body state due to the three-body physics. Mathematically, it is the residue of the two-body pole and its presence ensures that the on-shell (imaginary) part of the two-body Green function corresponds to the production of a fully dressed asymptotic two-body state with unit normalization.

Above the two-body threshold, the location of the two-body pole is given by,

$$k_{0\gamma} = \frac{1}{2} \sqrt{E^2 - 2(m_{\gamma_1}^2 + m_{\gamma_2}^2) + 2(m_{\gamma_1}^2 - m_{\gamma_2}^2)^2/E^2}. \quad (3.56)$$

The real part of the one-body self-energy $\Pi_\alpha(E)$ is calculated numerically using the identity

$$\mathcal{P} \int_0^\infty dk \frac{1}{k_{0\gamma}^2 - k^2} = 0. \quad (3.57)$$

The principal part integration of Eq. (3.51) is of the form,

$$\mathcal{P} \int_0^\infty dk \frac{h(k)}{E - g(k^2)}. \quad (3.58)$$

Its numerical evaluation is carried out by adding to this integral the term in Eq. (3.57) which is formally zero. If one defines the quantity $k_{0\gamma}$ from the condition that $g(k_{0\gamma}^2) = E$, then Eq. (3.58) can be equivalently written as

$$\begin{aligned} & \mathcal{P} \int_0^\infty dk \frac{h(k)}{E - g(k^2)} - \frac{\mathcal{P}}{g'(k_{0\gamma}^2)} \int_0^\infty dk \frac{h(k_{0\gamma})}{k_{0\gamma}^2 - k^2}, \\ &= \int_0^\infty dk \left(\frac{h(k)}{E - g(k^2)} - \frac{1}{g'(k_{0\gamma}^2)} \frac{h(k_{0\gamma})}{k_{0\gamma}^2 - k^2} \right). \end{aligned} \quad (3.59)$$

The resulting integrand is finite and integrable over the entire range of k , and can be calculated numerically using a variety of techniques.

In the CM frame, the one-body self-energy $\Pi_\alpha(E)$ depends only on the driving energy E . Thus, in this frame, the one-body self-energy is a complex function of E . Its dependence on the driving energy E arises *solely* from the energy dependence of the dressed two-body propagator $\tilde{G}_\gamma(k, E)$ and the dressed vertex $\tilde{V}_{\gamma 12 \alpha_1}(k, E)$, as required by unitarity. The details of the relations that arise from unitarity are explored in detail in Sec. III E.

The one-body mass counter term $\delta\Pi_\alpha$ is fixed by demanding that the elements of the one-body self-energies be identically zero when the driving energy $E = \mathcal{E}(m_{\alpha_1}, \mathbf{P})$. In the overall CM frame, the mass renormalization condition can then be written

$$\text{Re}(\Pi_\alpha(E))_{E \rightarrow m_{\alpha_1}} = 0. \quad (3.60)$$

In this framework, we assume that the finite size of the particles involved results in vertex form factors, such as $V_{\beta_1 \gamma 12}(k)$, which are assumed to fall off sufficiently rapidly in k to ensure the convergence of all integrals. Therefore, the counter term $\delta\Pi$ is finite and chosen such that Eq. (3.60) is satisfied.

D. Scattering amplitudes

Expressions for the scattering amplitudes are obtained in analogy to the self-energies obtained in the previous section. We will find however, that while the solution of the self-energies involved performing integrations, calculation of scattering amplitudes requires that one solve a linear integral equation.

Consider the form for the kernel K from Eq. (2.26). The most general form of the kernel is quite complicated when written in the partial-wave basis and will be addressed in a subsequent article. However, for the application to $\pi\pi$ scattering considered in Sec. IV, the two-body states $|\pi\pi\rangle$ and $|K\bar{K}\rangle$ are comprised of spinless particles and a simpler form of the kernel can be derived. The matrix element of the kernel is usually written $\langle \beta \mathbf{Q} \mathbf{q} | K | \alpha \mathbf{P} \mathbf{p} \rangle$ with the discrete quantum numbers being suppressed. These quantum numbers can be reinstated by recalling that

$$\begin{aligned} & |\alpha \mathbf{P} \mathbf{p} \rangle \longrightarrow \\ & |m_{\alpha_1} m_{\alpha_2} s_{\alpha_1} \lambda_{\alpha_1} s_{\alpha_2} \lambda_{\alpha_2} I_{\alpha_1} \kappa_{\alpha_1} I_{\alpha_2} \kappa_{\alpha_2} \mathbf{P} \mathbf{p} \rangle. \end{aligned} \quad (3.61)$$

In the CM frame and after dividing out the trivial factor of $(2\pi)^3 \delta(\mathbf{Q} - \mathbf{P})$ arising from total momentum conservation, one expands the kernel in a partial-wave basis,

$$\begin{aligned} \langle \beta_{12} \mathbf{q} | K | \alpha_{12} \mathbf{p} \rangle_{\mathbf{P}=0} &= \sum \langle I_{\beta_1} \kappa_{\beta_1} I_{\beta_2} \kappa_{\beta_2} | I \kappa \rangle \\ &\times Y_{L_\beta M_{L_\beta}}^*(\hat{\mathbf{q}}) \langle s_{\beta_1} \lambda_{\beta_1} s_{\beta_2} \lambda_{\beta_2} | S_\beta M_{S_\beta} \rangle \\ &\times \langle L_\beta M_{L_\beta} S_\beta M_{S_\beta} | J M_J \rangle K_{\beta\alpha}^J(q, p) \\ &\times \langle J M_J | L_\alpha M_{L_\alpha} S_\alpha M_{S_\alpha} \rangle \\ &\times \langle S_\alpha M_{S_\alpha} | s_{\alpha_1} \lambda_{\alpha_1} s_{\alpha_2} \lambda_{\alpha_2} \rangle Y_{L_\alpha M_{L_\alpha}}(\hat{\mathbf{p}}) \\ &\times \langle I \kappa | I_{\alpha_1} \kappa_{\alpha_1} I_{\alpha_2} \kappa_{\alpha_2} \rangle, \end{aligned} \quad (3.62)$$

where the summation is over $J, M_J, I, \kappa, L_\alpha, M_{L_\alpha}, S_\alpha, M_{S_\alpha}, L_\beta, M_{L_\beta}, S_\beta, M_{S_\beta}$. The partial-wave kernel is the reduced matrix element

$$\begin{aligned} & K_{\beta\alpha}^J(q, p) = \\ & \langle q m_{\beta_1} m_{\beta_2} S_\beta L_\beta s_{\beta_1} s_{\beta_2} | K^{JI} | p m_{\alpha_1} m_{\alpha_2} S_\alpha L_\alpha s_{\alpha_1} s_{\alpha_2} \rangle. \end{aligned} \quad (3.63)$$

In the following, the spherical reduced matrix element of the kernel will be simply denoted by $K_{\beta\alpha}^J(q, p)$. The single superscript J , which denotes the total angular momentum of the two-body system, is used to distinguish this element from the plane wave kernel $K_{\beta\alpha}(\mathbf{q}, \mathbf{p})$. The

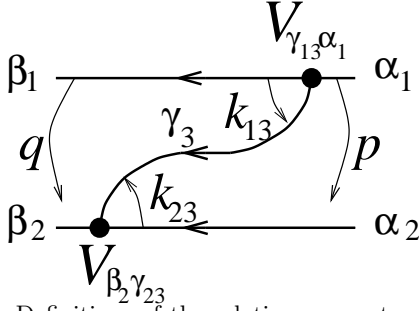


FIG. 11. Definitions of the relative momenta and particle labels for the kernel $K_{\beta\alpha}^{(1)}(q, p)$ given in Eq. (3.75).

partial-wave kernel can be obtained from the plane-wave kernel $K_{\beta\alpha}(\mathbf{q}, \mathbf{p})$ by

$$\begin{aligned}
K_{\beta\alpha}^J(q, p) &= \sum \int d\hat{q} d\hat{p} \langle JM_J | L_{\beta} M_{L_{\beta}} S_{\beta} M_{S_{\beta}} \rangle \\
&\times \langle S_{\beta} M_{S_{\beta}} | s_{\beta_1} \lambda_{\beta_1} s_{\beta_2} \lambda_{\beta_2} \rangle Y_{L_{\beta} M_{L_{\beta}}}(\mathbf{q}) \\
&\times \langle \beta \mathbf{q} | K | \alpha \mathbf{p} \rangle Y_{L_{\alpha} M_{L_{\alpha}}}^*(\mathbf{p}) \\
&\times \langle s_{\alpha_1} \lambda_{\alpha_1} s_{\alpha_2} \lambda_{\alpha_2} | S_{\alpha} M_{S_{\alpha}} \rangle \\
&\times \langle L_{\alpha} M_{L_{\alpha}} S_{\alpha} M_{S_{\alpha}} | JM_J \rangle, \quad (3.64)
\end{aligned}$$

and is comprised of two contributions,

$$K = K^{(1)} + K^{(2)} + K^{(4pt)}, \quad (3.65)$$

where

$$K^{(1)} = V_{23}^{(2)} G_3 V_{32}^{(1)}, \quad (3.66)$$

$$K^{(2)} = V_{23}^{(1)} G_3 V_{32}^{(2)}, \quad (3.67)$$

and $K^{(4pt)}$ is the part of the potential V_{22} that is *not* proportional to a Dirac δ -function in the relative momentum. This is the direct four-point coupling of four mesons, and it is depicted as four meson lines converging on a single point in Fig. 1. In Eq. (3.65), the parenthetical superscripts on the first two quantities refer to which of the two particles in the incoming state emits the exchanged particle, the superscript on the third quantity refers to the direct four-meson interaction. The exchanged particle is subsequently absorbed by the other particle in the outgoing state. The kernel $K^{(1)}$ is depicted in Fig. 11.

As described above, explicit expressions for the most general two-body kernels of Eqs. (3.66) and (3.67) in the spherical wave basis are complicated and not particularly enlightening. In the model application to $\pi\pi$ scattering considered in Sec. IV, the resulting kernel is relatively simple. The only matrix elements of V_{23} that are of interest in this application are those associated with the transitions of the forms $\pi\pi \rightarrow \pi\pi\rho$, $\pi\pi \rightarrow \pi\pi f_0$, $\pi\pi \rightarrow K\bar{K}\rho$ and $\pi\pi \rightarrow K\bar{K}f_0$, $\pi\pi \rightarrow \pi\bar{K}K^*$. In each of these hadron states, at least two of the three particles are spin-0 mesons. For these interactions, the potentials in V_{23} are of the form of Eq. (3.26) with

$$\begin{aligned}
\langle \gamma_{13} \mathbf{k}_{13} | V_{21} | \alpha_1 \rangle_{\mathbf{p}} &= \frac{(-1)^{s_{\gamma_3} - \lambda}}{\sqrt{2s_{\gamma_3} + 1}} \\
\sum_{\lambda} D_{\lambda_{\gamma_3}, \lambda}^{s_{\gamma_3}}(-\mathbf{k}, \mathbf{p}) k_{13}^{s_{\gamma_3}} Y_{s_{\gamma_3}, -\lambda}^*(\hat{\mathbf{k}}_{13}) V_{\gamma_{13}\alpha_1}(k_{13}). \quad (3.68)
\end{aligned}$$

The choice of momenta and labeling coincides with the interaction V_{32} depicted by the upper vertex in Fig. 11. These potentials take on very simple forms when the third particle in the intermediate state γ is either a scalar $s_{\gamma_3} = 0$, and

$$\langle \gamma_{13} \mathbf{k}_{13} | V_{21} | \alpha_1 \rangle_{\mathbf{p}} = \frac{1}{\sqrt{4\pi}} V_{\gamma_{13}\alpha_1}(k_{13}), \quad (3.69)$$

or, a vector $s_{\gamma_3} = 1$, in which case one can rewrite Eq. (3.68) in terms of two four-vectors $k_{\gamma_1}^{\mu}$ and $\varepsilon^{\mu}(\mathbf{p} - \mathbf{k}_{\gamma_1}, \lambda_{\gamma_3})$ as

$$\begin{aligned}
\langle \gamma_{13} \mathbf{k}_{13} | V_{21} | \alpha_1 \rangle_{\mathbf{p}} &= \frac{m_{\gamma_3}}{\mathcal{M}_{\gamma_{13}}(k_{13})} V_{\gamma_{13}\alpha_1}(k_{13}) \\
&\times \varepsilon_{\mu}(\mathbf{p} - \mathbf{k}_{\gamma_1}, \lambda_{\gamma_3}) k_{\gamma_1}^{\mu}. \quad (3.70)
\end{aligned}$$

In the frame moving with total momentum \mathbf{p} , particle γ_1 moves with three-momentum $\mathbf{k}_{\gamma_1} = \Lambda(\mathbf{p} \leftarrow 0) \mathbf{k}_{13}$ and its corresponding four-momentum is

$$k_{\gamma_1}^{\mu} = (\mathcal{E}(m_{\gamma_1}, \mathbf{k}_{\gamma_1}), \mathbf{k}_{\gamma_1}). \quad (3.71)$$

The polarization four-vector of the vector meson γ_3 is

$$\varepsilon^{\mu}(\mathbf{k}_{\gamma_3}, \lambda_{\gamma_3}) = (\varepsilon^0(\mathbf{k}_{\gamma_3}, \lambda_{\gamma_3}), \boldsymbol{\varepsilon}(\mathbf{k}_{\gamma_3}, \lambda_{\gamma_3})), \quad (3.72)$$

with $\mathbf{k}_{\gamma_3} = \mathbf{p} - \mathbf{k}_{\gamma_1}$, and

$$\boldsymbol{\varepsilon}(\mathbf{k}_{\gamma_3}, \lambda_{\gamma_3}) = \boldsymbol{\varepsilon}(0, \lambda_{\gamma_3}) + \frac{\mathbf{k}_{\gamma_3}}{m_{\gamma_3}} \frac{\boldsymbol{\varepsilon}(0, \lambda_{\gamma_3}) \cdot \mathbf{k}_{\gamma_3}}{m_{\gamma_3} + \mathcal{E}(m_{\gamma_3}, \mathbf{k}_{\gamma_3})}, \quad (3.73)$$

$$\varepsilon^0(\mathbf{k}_{\gamma_3}, \lambda_{\gamma_3}) = \frac{\boldsymbol{\varepsilon}(0, \lambda_{\gamma_3}) \cdot \mathbf{k}_{\gamma_3}}{m_{\gamma_3}}. \quad (3.74)$$

When these expressions for the matrix elements of V_{21} are substituted into Eq. (3.26) one has the necessary expressions for matrix elements of the potentials V_{32} . These are used in Eq. (3.66) to obtain an explicit form of the kernel $\langle \beta \mathbf{q}_1 \mathbf{q}_2 | K^{(1)} | \alpha \mathbf{p}_1 \mathbf{p}_2 \rangle$ in the plane wave basis. In the spherical wave basis, the kernel $K^{(1)}$ is given by

$$\begin{aligned}
K_{\beta\alpha}^{(1)J}(q, p) &= 2\pi \sum_{\gamma_{123}} \int_{-1}^{+1} dx \frac{P_J(x)}{4\pi} \frac{1}{2\mathcal{E}(m_{\gamma_3}, \mathbf{p} - \mathbf{q})} \\
&\times \frac{V_{\beta_2\gamma_{23}}(k_{23}) \mathcal{S}^{s_{\gamma_3}}(\mathbf{q}, \mathbf{p}) V_{\gamma_{13}\alpha_1}(k_{13})}{E - \mathcal{M}_{\gamma_{123}}(\mathbf{q}, -\mathbf{p}, \mathbf{p} - \mathbf{q}) + i\epsilon}, \quad (3.75)
\end{aligned}$$

where

$$\begin{aligned}
\mathcal{S}^{s_{\gamma_3}=0}(\mathbf{q}, \mathbf{p}) &= 1, \\
\mathcal{S}^{s_{\gamma_3}=1}(\mathbf{q}, \mathbf{p}) &= q_{\beta_1}^{\mu} \left(\frac{-m_{\gamma_3}^2 g_{\mu\nu} + k_{\gamma_3\mu} k_{\gamma_3\nu}}{\mathcal{M}_{\gamma_{23}}(k_{23}) \mathcal{M}_{\gamma_{13}}(k_{13})} \right) p_{\alpha_2}^{\nu}, \quad (3.76)
\end{aligned}$$

for scalar exchanges ($s_{\gamma_3} = 0$) and vector exchanges ($s_{\gamma_3} = 1$), respectively, and $P_J(x)$ are the usual Legendre polynomials in $x = \mathbf{p} \cdot \mathbf{q} / pq$. The three four-momenta appearing in Eq. (3.75) are

$$\begin{aligned} q_{\beta_1}^\mu &= (\mathcal{E}(m_{\beta_1}, \mathbf{q}), \mathbf{q}), \\ p_{\alpha_2}^\mu &= (\mathcal{E}(m_{\alpha_2}, -\mathbf{p}), -\mathbf{p}), \\ k_{\gamma_3}^\mu &= (\mathcal{E}(m_{\gamma_3}, \mathbf{p} - \mathbf{q}), \mathbf{p} - \mathbf{q}). \end{aligned} \quad (3.77)$$

Expressions corresponding to the matrix elements of $K_{\beta\alpha}^{(2)}(q, p)$ can be obtained in a similar manner.

Once specific forms of the model vertex form factors $V_{\gamma_{13}\alpha_1}(k_{13})$ and $V_{\beta_2\gamma_{23}}(k_{23})$ are provided and substituted into Eq. (3.75), the matrix elements of the kernel K are computed numerically. The imaginary part of the kernel arises from the pole contribution of the three-body Green function $G_{\gamma_{123}}$ in Eq. (3.75). The pole is encountered by the angular integration at the value of $x = x_{0\gamma}$ for which the three-particle intermediate state γ is on-energy-shell. The three-body pole is located at

$$\begin{aligned} x_{0\gamma} &= \frac{1}{2pq} ((E - \mathcal{E}(m_{\gamma_1}, \mathbf{q}) - \mathcal{E}(m_{\gamma_2}, -\mathbf{p}))^2 \\ &\quad - m_{\gamma_3}^2 - q^2 - p^2), \end{aligned} \quad (3.78)$$

for CM energies satisfying

$$E > \mathcal{E}(m_{\gamma_1}, \mathbf{q}) + \mathcal{E}(m_{\gamma_2}, -\mathbf{p}). \quad (3.79)$$

When these criteria are met, the integrand is complex-valued and the imaginary part of Eq. (3.75) is proportional to $\delta(x - x_{0\gamma})$. Hence, the imaginary part of the kernel $K_{\beta\alpha}^J(q, p)$ can be evaluated analytically.

The real part of the kernel is evaluated numerically using a simple integration routine and a finite value for the adiabatic energy scale ϵ . The resulting spherical wave kernel $K_{\beta\alpha}^J(q, p)$ is finite, but has branch cuts associated with any open three-body channels.

Once the kernel has been evaluated numerically, one can proceed to solve the integral equation in Eq. (2.42) for the scattering amplitude $t^{(2)}$. In the CM frame, the integral equation for the partial-wave scattering amplitude $t_{\beta\alpha}^{(2)J}(q, p)$ has the form

$$\begin{aligned} t_{\beta\alpha}^{(2)J}(q, p) &= K_{\beta\alpha}^J(q, p) + \sum_{\gamma_{12}} \int_0^\infty dk a_{\gamma_{12}}(k, 0) \\ &\quad \times K_{\beta\gamma}^J(q, k) \tilde{G}_\gamma(k, E) t_{\gamma\alpha}^{(2)J}(k, p), \end{aligned} \quad (3.80)$$

where $a_{\gamma_{12}}(k, 0)$ is the phase space factor of Eq. (3.52) for the two-body system. Obtaining the solution of this integral equation may be complicated by the presence of a pole in the two-body propagator $\tilde{G}_\gamma(k)$. The method used to solve this integral equation is adapted from Ref. [19]. Above the two-particle threshold $E > m_{\gamma_1} + m_{\gamma_2}$, the Green function

$$\tilde{G}_\gamma(k, E) = (E - \mathcal{M}_{\gamma_{12}}(k) - \Sigma_\gamma(k, E))^{-1} \quad (3.81)$$

has a pole at $k_{0\gamma}$, where $k_{0\gamma}$ is a function of the driving energy E and is the solution to $\mathcal{M}_{\gamma_{12}}(k_{0\gamma}) = E$, given by

$$k_{0\gamma} = \frac{E}{2} \sqrt{1 - \frac{2(m_{\gamma_1}^2 + m_{\gamma_2}^2)}{E^2} + \left[\frac{m_{\gamma_1}^2 - m_{\gamma_2}^2}{E^2} \right]^2}. \quad (3.82)$$

The Green function can then be rewritten as a (real) principal part, plus an imaginary part containing a delta-function, *i.e.*

$$\tilde{G}_\gamma(k, E) = \mathcal{P}\tilde{G}_\gamma(k, E) - \frac{i\pi z_\gamma}{2k_{0\gamma}\rho_{\gamma_{12}}(k_{0\gamma})} \delta(k - k_{0\gamma}). \quad (3.83)$$

In Eq. (3.83), \mathcal{P} denotes the principal part and z_γ is the residue of $\tilde{G}_\gamma(k_{0\gamma}, E)$, defined by Eq. (3.55). The integral equation for $t^{(2)}$ is then,

$$\begin{aligned} t_{\beta\alpha}^{(2)J}(q, p) &= K_{\beta\alpha}^J(q, p) \\ &+ \sum_{\gamma_{12}} \mathcal{P} \int_0^\infty dk a_{\gamma_{12}}(k, 0) K_{\beta\gamma}^J(q, k) \tilde{G}_\gamma(k, E) t_{\gamma\alpha}^{(2)J}(k, p) \\ &- i\pi \sum_{\gamma_{12}} \frac{a_{\gamma_{12}}(k_{0\gamma}, 0) z_\gamma}{2k_{0\gamma}\rho_{\gamma_{12}}(k_{0\gamma})} K_{\beta\gamma}^J(q, k_{0\gamma}) t_{\gamma\alpha}^{(2)J}(k_{0\gamma}, p) \end{aligned} \quad (3.84)$$

Following Ref. [19], one adds to the principal part integral a term proportional to

$$\zeta_\gamma = \mathcal{P} \int_0^\infty dk \frac{1}{k^2 - k_{0\gamma}^2}, \quad (3.85)$$

whose contribution to the integral equation of Eq. (3.84) is identically zero. However, the addition of this term to Eq. (3.84) produces a zero at the pole position $k_{0\gamma}$, thereby making the integration amenable to numerical evaluation. To see why, observe that when one expands the dressed Green function $\tilde{G}_\gamma(k, E)$ in powers of $k^2 - k_{0\gamma}^2$, one obtains

$$\tilde{G}_\gamma(k, E) = \frac{-1}{k^2 - k_{0\gamma}^2} \frac{z_\gamma}{\rho_{\gamma_{12}}(k_{0\gamma})} + \dots, \quad (3.86)$$

where we neglect terms which are finite in the limit that $k^2 \rightarrow k_{0\gamma}^2$. With a judicious choice of coefficients for the function ζ_γ , the two integrands cancel exactly at the two-particle pole position $k = k_{0\gamma}$ and the two principal-parts integrations can be replaced by a single, canonical integration. The two-particle scattering amplitude $t^{(2)}$ is then given by

$$\begin{aligned} t_{\beta\alpha}^{(2)J}(q, p) &= K_{\beta\alpha}^J(q, p) \\ &+ \sum_{\gamma_{12}} \int_0^\infty dk \left[a_{\gamma_{12}}(k, 0) K_{\beta\gamma}^J(q, k) \tilde{G}_\gamma(k, E) t_{\gamma\alpha}^{(2)J}(k, p) \right. \\ &\quad \left. + \frac{a_{\gamma_{12}}(k_{0\gamma}, 0) z_\gamma}{\rho_{\gamma_{12}}(k_{0\gamma})} \frac{K_{\beta\gamma}^J(q, k_{0\gamma})}{k^2 - k_{0\gamma}^2} t_{\gamma\alpha}^{(2)J}(k_{0\gamma}, p) \right] \\ &- i\pi \sum_{\gamma_{12}} \frac{a_{\gamma_{12}}(k_{0\gamma}, 0) z_\gamma}{2k_{0\gamma}\rho_{\gamma_{12}}(k_{0\gamma})} K_{\beta\gamma}^J(q, k_{0\gamma}) t_{\gamma\alpha}^{(2)J}(k_{0\gamma}, p). \end{aligned} \quad (3.87)$$

The integral equation Eq. (3.87) contains an integral over the continuous variable k , plus a discrete contribution at the point $k_{0\gamma}$. To proceed, this is converted into a matrix equation, by introducing a set of momentum mesh points and associated weights $\{p_i, w_i\}$ for $i = 1, \dots, N$. To accommodate the contribution at $k_{0\gamma}$, an additional momentum value $p_i = k_{0\gamma}$ with $i = N+1$ is introduced to the mesh for each channel γ . Matrices are constructed for the amplitudes in Eq. (3.87), whose matrix elements are the functions evaluated at momenta in the augmented set of mesh points. The result is that the integral equation is now a matrix equation with a double summation. The first index $k = 1, \dots, N+1$ runs over the momentum mesh points, while the second index runs over the two-particle channels $\gamma = \gamma_{12}$. The matrix equation is

$$t_{\beta j \alpha i}^{(2)} = K_{\beta j \alpha i} + \sum_{\gamma} \sum_{k=1}^{N+1} A_{\beta j \gamma k} t_{\gamma k \alpha i}^{(2)}, \quad (3.88)$$

where for $j, k = 1, \dots, N$ one has

$$A_{\beta j \gamma k} = a_{\gamma_{12}}(p_k) K_{\beta \gamma}(p_j, p_k) \tilde{G}_{\gamma}(p_k, E) w_k, \quad (3.89)$$

and for $j = 1, \dots, N$ and $k = N+1$ one has

$$A_{\beta j \gamma(N+1)} = \frac{a_{\gamma_{12}}(k_{0\gamma}) z_{\gamma}}{\rho_{\gamma_{12}}(k_{0\gamma})} K_{\beta \gamma}(p_j, k_{0\gamma}) \zeta_{\gamma} - i\pi \frac{a_{\gamma_{12}}(k_{0\gamma}) z_{\gamma}}{2k_{0\gamma} \rho_{\gamma_{12}}(k_{0\gamma})} K_{\beta \gamma}^J(p_j, k_{0\gamma}). \quad (3.90)$$

The solution to the integral equation is obtained by matrix inversion, which yields.

$$\begin{aligned} t_{\beta j \alpha i}^{(2)} &= \sum_{\gamma} \sum_{k=1}^{N+1} (\delta_{\gamma \beta} \delta_{kj} - A_{\gamma k \beta j})^{-1} K_{\gamma k \alpha i}, \\ &= \sum_{\gamma, k} (\mathcal{I} - \mathcal{A})_{\beta j \gamma k}^{-1} K_{\gamma k \alpha i}, \end{aligned} \quad (3.91)$$

where the unit matrix \mathcal{I} is diagonal in both channel indices and momentum mesh points. In practice, this matrix inversion is straight-forward to carry out numerically. It is convenient to rewrite Eq. (3.91) in terms of continuous variables,

$$t_{\beta \alpha}^{(2)J}(q, p) = \sum_{\gamma_{12}} \int_0^{\infty} dk a_{\gamma_{12}}(k, 0) \Omega_{\beta \gamma}^{(2)J}(q, k) K_{\gamma \alpha}^J(k, p), \quad (3.92)$$

where we have introduced the amplitude,

$$\frac{(\mathcal{I} - \mathcal{A})_{\beta j \alpha i}^{-1}}{w_i a_{\alpha_{12}}(p_i, 0)} \longrightarrow \Omega_{\beta \alpha}^{(2)J}(q, p), \quad (3.93)$$

referred to as the *two-body* Moller amplitude. The plane-wave basis matrix element for this amplitude can be reconstructed in a manner analogous to the procedure we

employed with the two-particle kernel K in Eq. (3.62). Using this technique it is easy to reconstruct an operator form of Eq. (3.92),

$$t^{(2)} = \Omega^{(2)} K. \quad (3.94)$$

There are two important observations to be made concerning the two-body Moller amplitude $\Omega^{(2)}$. First, the operator $\Omega^{(2)}$ is not symmetric. It is clear from Eq. (3.94) that observed from the left, the two-body Moller operator $\Omega^{(2)}$ appears to be an amputated vertex function (that is, it behaves like a potential V or T -matrix). When observed from the right, it appears to be an unamputated Green function.

Second, the two-body Moller operator $\Omega^{(2)}$ employed herein is *not* the same as the Moller operator Ω that is employed in general analyses of scattering theory [20]. The canonical definition of the Moller operator Ω is that it transforms the *full* potential V from Eq. (2.19) into the *full* T -matrix of Eq. (2.13); that is, $T = \Omega V$. In contrast, the two-body Moller operator $\Omega^{(2)}$ as defined in Eq. (3.94), is a transformation that maps the two-body kernel K into the two-body part $t^{(2)}$ of the T_{22} -matrix. The purpose for introducing the two-body Moller operator $\Omega^{(2)}$ will become clear in Sec. III E when the unitarity of the framework is demonstrated.

In Sec. II, the two-body scattering amplitude T_{22} was separated into a sum of two pieces $t^{(1)}$ and $t^{(2)}$. Now that we have solved for the term $t^{(2)}$, we shall proceed to obtain an explicit expression for the two-body scattering amplitude $t^{(1)}$. It is given in Eq. (2.41) by

$$t^{(1)} = \tilde{V}_{21} \tilde{G}_1 \tilde{V}_{12}. \quad (3.95)$$

The solution of the intermediate dressed one-body Green function \tilde{G}_1 was given in Sec. III C 2. All that remains is to determine the form of the dressed vertices \tilde{V}_{12} and \tilde{V}_{21} . The dressed vertex can be written as

$$\langle \beta \mathbf{q} \mathbf{Q} | \tilde{V}_{21} | \alpha \mathbf{P} \rangle = (2\pi)^3 \delta(\mathbf{Q} - \mathbf{P}) \langle \beta_{12} \mathbf{q} | \tilde{V}_{21} | \alpha_1 \rangle_{\mathbf{P}}, \quad (3.96)$$

with the matrix element, evaluated in the CM frame,

$$\begin{aligned} \langle \beta_{12} \mathbf{q} | \tilde{V}_{21} | \alpha_1 \rangle_{\mathbf{P}=0} &= \sum \langle L_{\beta} M_{L_{\beta}} S_{\beta} M_{S_{\beta}} | s_{\alpha_1} \lambda_{\alpha_1} \rangle \\ &\times \langle s_{\beta_1} \lambda_{\beta_1} s_{\beta_2} \lambda_{\beta_2} | S_{\beta} M_{S_{\beta}} \rangle \\ &\times \langle I_{\beta_1} \kappa_{\beta_1} I_{\beta_2} \kappa_{\beta_2} | I_{\alpha_1} \kappa_{\alpha_1} \rangle \\ &\times Y_{L_{\beta} M_{L_{\beta}}}^*(\hat{\mathbf{q}}) \tilde{V}_{\beta_{12} \alpha_1}(q). \end{aligned} \quad (3.97)$$

The summation in Eq. (3.97) runs over L_{β} , $M_{L_{\beta}}$, S_{β} , and $M_{S_{\beta}}$. The integral equation for the dressed vertex is obtained from the transpose of Eq. (2.34) with the insertion of a complete set of two-body intermediate states $|\gamma \mathbf{K} \mathbf{k}\rangle$,

$$\begin{aligned} \tilde{V}_{\beta_{12} \alpha_1}(q) &= V_{\beta_{12} \alpha_1}(q) + \sum_{\gamma_{12}} \int_0^{\infty} dk a_{\gamma_{12}}(k, 0) \\ &\times K_{\beta \gamma}^{J=s_{\alpha_1}}(q, k) \tilde{G}_{\gamma}(k, E) \tilde{V}_{\gamma_{12} \alpha_1}(k) \end{aligned} \quad (3.98)$$

The similarity between this integral equation and the integral equation of Eq. (3.80) with $J = s_{\alpha_1}$ which determines $t^{(2)}$ is evident. Hence it follows that the solution to Eq. (3.98) is just

$$\tilde{V}_{\beta_{12}\alpha_1}(q) = \sum_{\gamma_{12}} \int_0^\infty dk a_{\gamma_{12}}(k, 0) \Omega_{\beta\gamma}^{(2)J=s_{\alpha_1}}(q, k) V_{\gamma_{12}\alpha_1}(k). \quad (3.99)$$

The final piece of the two-body scattering amplitude is obtained upon inserting a complete set of one-particle states into Eq. (2.41). One finds

$$t_{\beta\alpha}^{(1)J}(q, p) = \sum_{\gamma_1\gamma_2} \frac{\tilde{V}_{\beta_{12}\gamma_1}^J(q) \tilde{G}_{\gamma_1\gamma_2}(E) \tilde{V}_{\gamma_1\alpha_{12}}^J(p)}{2\sqrt{m_{\gamma_1}, m_{\gamma_2}}} \quad (3.100)$$

The two-body scattering amplitude T_{22} is obtained by adding this to $t^{(2)}$ according to Eq. (2.40).

In the previous sections, we have demonstrated that the explicit solution to the scattering problem involving one-, two-, and three-body states can be obtained by performing several integrations and one matrix inversion. The latter is necessary to determine the two-body Moller amplitude $\Omega_{\beta\alpha}^{(2)J}(q, p)$. Next, in Sec. III E, it is demonstrated that the numerical approach described above does in fact maintain the unitarity of the theory to better than one part in ten thousand. In Sec. IV, the framework is applied to the study of $\pi\pi$ scattering.

E. Demonstration of unitarity

The unitarity condition (or optical theorem) can be derived directly from the formal LSE

$$T = V + VGT, \quad (3.101)$$

by taking the hermitian transpose and from it, subtracting the original LSE. Since the potential matrix V is hermitian, one has

$$T - T^\dagger = T^\dagger(G - G^\dagger)T. \quad (3.102)$$

In the following, we will concentrate on the elastic two-particle scattering sector of the theory. Hence, we retain only the diagonal terms from the above relation which do not vanish when evaluated between two-particle states. Written in terms of the matrix elements of Eqs. (2.20) and (2.21), these are

$$2i\text{Im} T_{22} = T_{21}^\dagger(G_1 - G_1^\dagger)T_{12} + T_{22}^\dagger(G_2 - G_2^\dagger)T_{22} + T_{23}^\dagger(G_3 - G_3^\dagger)T_{32}. \quad (3.103)$$

We collect these contributions into the following terms,

$$U^{(\text{tot})} = 2i\text{Im}T_{22}, \quad (3.104)$$

$$U^{(1)} = T_{21}^\dagger(G_1 - G_1^\dagger)T_{12}, \quad (3.105)$$

$$U^{(2)} = T_{22}^\dagger(G_2 - G_2^\dagger)T_{22}, \quad (3.106)$$

$$U^{(3)} = T_{23}^\dagger(G_3 - G_3^\dagger)T_{32}. \quad (3.107)$$

The unitarity condition of Eq. (3.103) can be rewritten as

$$U^{(\text{tot})} - U^{(1)} - U^{(2)} - U^{(3)} = \delta U, \quad (3.108)$$

with δU representing the violation to unitarity. In a unitary theory, $\delta U = 0$. Equation (3.108) represents the statement of the conservation of probability in the two-body scattering problem.

The unitarity of the framework is explored by evaluating each of the above contributions in the left-hand side of Eq. (3.108). First, we examine the term in Eq. (3.104). The formal solution for the two-body scattering amplitude T_{22} is given in Eq. (2.40),

$$T_{22} = G_2^{-1} \tilde{G}_2(t^{(1)} + t^{(2)}) \tilde{G}_2 G_2^{-1} + G_2^{-1} \tilde{G}_2 \Sigma. \quad (3.109)$$

The final term is zero for on-energy-shell states and will be neglected in the following. Evaluating this between two-particle states, the result involves the ratio of dressed to bare two-body Green functions,

$$G_\alpha^{-1}(p, E) \tilde{G}_\alpha(p, E) = \frac{E - \mathcal{M}_{\alpha_{12}}(p) + i\epsilon}{E - \mathcal{M}_{\alpha_{12}}(p) - \Sigma_\alpha(p, E) + i\epsilon}. \quad (3.110)$$

One must consider two cases in order to evaluate this ratio. The first case is for unstable two-body states. Then, the two-body on-energy-shell self-energy $\Sigma_\alpha(p, \mathcal{M}_\alpha(p)) \neq 0$ has a non-zero imaginary component. It follows that in the limit $E \rightarrow \mathcal{M}_{\alpha_{12}}(p)$, the ratio of Green functions in Eq. (3.110) is zero. Hence, the T_{22} -matrix element in Eq. (3.104) vanishes for on-energy-shell two-particle states.

This is a general feature of the present framework. One can prove that *all* T -matrix elements that connect to unstable two-body states $|\alpha\mathbf{p}\mathbf{P}\rangle$ will *vanish* for on-shell energies $E = \mathcal{E}(\mathcal{M}_{\alpha_{12}}(p), \mathbf{P})$. In essence, unstable states simply decouple from the stable states and they can never be produced as asymptotic states; they seem to *evaporate* from the set of observable states. Of course, their effect on a scattering process is still felt through intermediate quantum fluctuations.

In the case of a stable two-body state, our choice of two-particle mass counter-terms from Eq. (3.47) implies that in taking the on-energy-shell limit $E \rightarrow \mathcal{M}_\alpha(p)$ in the CM frame, the two-body self-energy $\Sigma_\alpha(\mathbf{p}, E) = 0$. Recalling that in this framework, the adiabatic switching scale ϵ is small, but *finite*, it follows that the ratio Eq. (3.110) goes to 1 in the on-energy-shell limit.

The matrix element of $U^{(\text{tot})}$ in the partial-wave basis is defined by

$$\begin{aligned} \langle \beta \mathbf{q} \mathbf{Q} | U^{(\text{tot})} | \alpha \mathbf{P} \mathbf{P} \rangle &= (2\pi)^3 \delta(\mathbf{Q} - \mathbf{P}) \sum_{JM} Y_{JM}^*(\hat{\mathbf{q}}) \\ &\times U_{\beta\alpha}^{(\text{tot})J}(q, p) Y_{JM}(\hat{\mathbf{p}}), \end{aligned} \quad (3.111)$$

and is given by,

$$U_{\beta\alpha}^{(\text{tot})J}(q, p) = 2i \text{Im} \left(t_{\beta\alpha}^{(1)J}(q, p) + t_{\beta\alpha}^{(2)J}(q, p) \right) \quad (3.112)$$

The diagonal, on-energy-shell element $U_{\alpha\alpha}^{(\text{tot})J}(p_0, p_0)$ represents the total loss of flux from the incoming state α . It is the shadow contribution in the optical theorem.

Next, we obtain an explicit relation for $U^{(1)}$, representing the amount of lost incoming two-particle flux that appears in outgoing one-particle states. The formal expression for T_{21} from Eq. (2.35) is

$$T_{21} = G_2^{-1} \tilde{G}_2 \tilde{V}_{21} \tilde{G}_1 G_1^{-1}. \quad (3.113)$$

Upon inserting this into Eq. (3.105) and evaluating it between two-particle states, one obtains an expression for $\langle \beta \mathbf{Q} \mathbf{q} | U^{(1)} | \alpha \mathbf{P} \mathbf{P} \rangle$. However, one can show that for energies above the two-particle scattering threshold, the matrix elements of T_{21} are identically zero. From this it follows that

$$U_{\beta\alpha}^{(1)J}(q, p) = 0. \quad (3.114)$$

To prove this, consider the matrix elements of Eq. (3.113),

$$\begin{aligned} \langle \beta \mathbf{Q} \mathbf{q} | T_{21} | \alpha \mathbf{P} \rangle &= (2\pi)^3 \delta(\mathbf{Q} - \mathbf{P}) \langle \beta_{12} \mathbf{q} | \tilde{V}_{21} | \alpha_1 \rangle_{\mathbf{P}} \\ &\times G_{\beta}^{-1}(q, E) \tilde{G}_{\beta}(q, E) \\ &\times \tilde{G}_{\alpha}(E) G_{\alpha}^{-1}(E), \end{aligned} \quad (3.115)$$

where we have used Eq. (3.96). The above matrix element is proportional to the product of dressed and bare one-particle and two-particle Green functions. The ratio of two-particle Green functions was discussed above, and assuming the state $|\beta \mathbf{Q} \mathbf{q}\rangle$ is stable, it is equal to 1. In the CM frame, the ratio of one-body Green functions is

$$\tilde{G}_{\alpha}(E) G_{\alpha}^{-1}(E) = \frac{E - m_{\alpha_1} + i\epsilon}{E - m_{\alpha_1} - \Pi_{\alpha}(E) + i\epsilon}. \quad (3.116)$$

For energies E above an open two-particle channel threshold, the one-body state $|\alpha \mathbf{P}\rangle$ must be unstable, since it couples to, and therefore can decay into, the open two-particle channel. It follows that the one-body self-energy $\Pi_{\alpha}(E)$ has a finite imaginary part at the energy $E = m_{\alpha_1}$ and in the limit that $E \rightarrow m_{\alpha_1}$, the product in Eq. (3.116) must be zero; equation (3.114) follows. The interpretation is clear. None of the incoming two-particle flux can be lost to one-body channels since such channels are either unstable or have energies that are below the two-body threshold energy (and are therefore inaccessible to two-body scattering).

A corollary to this proof is that *only* for energies E that are below *all* two-particle thresholds in a given channel can $U^{(1)}$ be different from zero. Such a situation does occur in strong interaction physics. Two examples are the channels $J^P = 0^-$ and $J^P = \frac{1}{2}^+$, for which the pion and proton are stable one-particle states. Nonetheless, even for these channels, the *stable* one-body states are necessarily below the two-particle thresholds and so can not be produced as a real final state, and do not contribute to the unitarity condition in Eq. (3.108). We conclude that Eq. (3.114) is an identity for all two-body scattering processes.

Continuing, we now consider the loss of flux that appears as outgoing two-body states. From Eq. (3.106), we obtain

$$\begin{aligned} \langle \beta \mathbf{Q} \mathbf{q} | U^{(2)} | \alpha \mathbf{P} \mathbf{P} \rangle &= (2\pi)^3 \delta(\mathbf{Q} - \mathbf{P}) \langle \beta_{12} \mathbf{q} | (t^{(1)} + t^{(2)})^{\dagger} \\ &\times ((G_2^{-1} \tilde{G}_2)^* \tilde{G}_2 - \tilde{G}_2^* (\tilde{G}_2 G_2^{-1})) \\ &\times (t^{(1)} + t^{(2)}) | \alpha_{12} \mathbf{P} \rangle_{\mathbf{P}}. \end{aligned} \quad (3.117)$$

Inserting a complete set of two-body states into this equation and projecting out the J^{th} partial wave, one obtains

$$\begin{aligned} U_{\beta\alpha}^{(2)J}(q, p) &= \sum_{\gamma_{12}} \int_0^{\infty} dk a_{\gamma_{12}}(k, 0) \\ &\times (t_{\beta\gamma}^{(1)J}(q, k) + t_{\beta\gamma}^{(2)J}(q, k))^{\dagger} \\ &\times 2\pi i \delta(E - \mathcal{M}_{\gamma_{12}}(k) - \Sigma_{\gamma}(k, E)) \\ &\times (t_{\gamma\alpha}^{(1)J}(k, p) + t_{\gamma\alpha}^{(2)J}(k, p)). \end{aligned} \quad (3.118)$$

The δ -function allows the integral in Eq. (3.118) to be done analytically, yielding

$$\begin{aligned} U_{\beta\alpha}^{(2)J}(q, p) &= \sum_{\gamma_{12}} \frac{ik_{0\gamma} z_{\gamma}}{2\pi} (t_{\beta\gamma}^{(1)}(q, k_{0\gamma}) + t_{\beta\gamma}^{(2)}(q, k_{0\gamma}))^{\dagger} \\ &\times (t_{\gamma\alpha}^{(1)}(k_{0\gamma}, p) + t_{\gamma\alpha}^{(2)}(k_{0\gamma}, p)) \end{aligned} \quad (3.119)$$

where z_{γ} is the wave function renormalization for the two-body state γ and the sum over intermediate two-particle states is restricted to just those states that are above threshold; that is, the sum is over all γ for which there exists a $k_{0\gamma} \geq 0$ such that $\mathcal{M}_{\gamma_{12}}(k_{0\gamma}) = E$. The diagonal on-energy-shell elements of the resulting quantity $U_{\alpha\alpha}^{(2)J}(p_0, p_0)$ in Eq. (3.119) represent the amount of incoming two-particle flux that ends up as outgoing two-particle states. This includes both the elastic scattering flux, which appears at non-forward angles, as well as flux to other two-particle channels.

The final term in Eq. (3.108) is the most complicated. It accounts for the loss of incoming two-particle flux that appears asymptotic, outgoing three-particle states. The difficulty in deriving this term arises from the complexity of the T_{32} matrix, which is of the form,

$$T_{32} = V_{32} (1 + \tilde{G}_2 t^{(1)} + \tilde{G}_2 t^{(2)}) \tilde{G}_2 G_2^{-1}. \quad (3.120)$$

One may observe that the above equation contains the expression $\Omega^{(2)T} = 1 + \tilde{G}_2 t^{(2)}$, where the superscript T refers to the transpose of the operator. The operator $\Omega^{(2)}$ is, in fact, the two-particle Moller operator defined by Eq. (3.94). It is convenient to collect all of the terms in the above equation together and define the transpose of a *new* Moller operator, $\tilde{\Omega}^T = \tilde{G}_2 t^{(1)} + \Omega^{(2)T}$. Then, the expression for the T_{32} matrix simplifies to

$$T_{32} = V_{32} \tilde{\Omega}^T \tilde{G}_2 G_2^{-1}. \quad (3.121)$$

Inserting this into Eq. (3.107) gives,

$$\begin{aligned} \langle \beta \mathbf{Q} \mathbf{q} | U^{(3)} | \alpha \mathbf{P} \mathbf{p} \rangle &= (2\pi)^3 \delta(\mathbf{Q} - \mathbf{P}) \\ &\times \langle \beta_{12} \mathbf{q} | \tilde{\Omega}^* V_{23}^* (G_3 - G_3^*) V_{32} \tilde{\Omega}^T | \alpha_{12} \mathbf{p} \rangle_{\mathbf{P}}. \end{aligned} \quad (3.122)$$

One can proceed as we did with the two-body case and rewrite the difference of the two propagators as an energy-conserving delta function. However, it is more illuminating to consider the following. In the above equation, there is a difference of two operator products,

$$\begin{aligned} V_{23}^* G_3 V_{32} - V_{23}^* G_3^* V_{32} &= V_{23} G_3 V_{32} - (V_{23} G_3 V_{32})^* \\ &= (\Sigma + K) - (\Sigma + K)^* \\ &= 2i \text{Im}(\Sigma + K), \end{aligned} \quad (3.123)$$

where we use the fact that the matrix elements of the potential V are real. Inserting a complete set of states, one can rewrite $U^{(3)}$ as a sum of two terms,

$$U^{(3)} = U^{(3\Sigma)} + U^{(3K)}, \quad (3.124)$$

where the partial-wave decomposition of these is

$$\begin{aligned} U_{\beta\alpha}^{(3\Sigma)J}(q, p) &= \sum_{\gamma_{12}} \int_0^\infty dk a_{\gamma_{12}}(k, 0) \tilde{\Omega}_{\beta\gamma}^{J*}(q, k) \\ &\times \text{Im} \Sigma_\gamma(k, E) \tilde{\Omega}_{\gamma\alpha}^{JT}(k, p), \end{aligned} \quad (3.125)$$

and

$$\begin{aligned} U_{\beta\alpha}^{(3K)J}(q, p) &= \sum_{\gamma_{12}, \mu_{12}} \int_0^\infty dk a_{\gamma_{12}}(k, 0) \int_0^\infty dk' a_{\mu_{12}}(k', 0) \\ &\times \left(\tilde{\Omega}_{\beta\mu}^{J*}(q, k') \text{Im} K_{\mu\gamma}^J(k', k) \tilde{\Omega}_{\gamma\alpha}^{JT}(k, p) \right). \end{aligned} \quad (3.126)$$

Finally, we have arrived at the desired unitarity condition,

$$\begin{aligned} \delta U_{\beta\alpha}^J(q, p) &= U_{\beta\alpha}^{(\text{tot})J}(q, p) - U_{\beta\alpha}^{(1)J}(q, p) - U_{\beta\alpha}^{(2)J}(p_0, p_0) \\ &\quad - U_{\beta\alpha}^{(3\Sigma)J}(q, p) - U_{\beta\alpha}^{(3K)J}(q, p). \end{aligned} \quad (3.127)$$

The derivation of Eq. (3.127) depends on two conditions. The first is that the Hilbert space be truncated to include only one-, two-, and three-body states. (Otherwise, Eq. (3.127) would include contributions from states with higher numbers of particles.) The second condition is that the matrix elements of the potential

V in Eq. (2.19) are all real and time-independent. The latter of these two conditions is violated since a small time-dependence proportional to $e^{-\epsilon|t|}$ was introduced in Eq. (2.16). This time-dependence results in a violation of the unitarity condition in Eq. (3.127) that is proportional to ϵ , and so, one expects $\delta U_{\beta\alpha}^J(q, p) \sim \epsilon$. Another source of unitarity violation results from numerical computations which always suffer from round-off errors and finite mesh sizes. However, such violations are independent of the adiabatic-switching parameter ϵ . It follows that for small-enough values of ϵ , $\delta U_{\beta\alpha}^J(q, p)$ will become independent of ϵ . For this range of ϵ , the magnitude of $\delta U_{\beta\alpha}^J(q, p)$ provides an indication of the accuracy of the numerical methods employed.

To help visualize the role of unitarity in the framework, it is convenient to define the following ratios,

$$r^{(i)J} = \frac{U_{\alpha\alpha}^{(\text{tot})J}(p_0, p_0) - \sum_{n=1}^i U_{\alpha\alpha}^{(n)J}(p_0, p_0)}{U_{\alpha\alpha}^{(\text{tot})J}(p_0, p_0)}, \quad (3.128)$$

where p_0 is the on-energy-shell momentum of the two-body state $|\alpha\rangle$ satisfying $\mathcal{M}_{\alpha_{12}}(p_0) = E$. The quantity $r^{(i)J}$ represents the fraction of the forward flux, for two-body scattering with angular momentum J , which is lost to all states with numbers of particles $n > i$. Since there can be no stable one-body states above the two-pion threshold, $U_{\pi\pi}^{(1)}(p_0, p_0) = 0$ as given in Eq. (3.114), we see that $r^{(1)J} = 1$. That is, all of the two-pion flux missing from the shadow region must be accounted for elsewhere. The quantity $r^{(2)J}$ gives the fraction of flux lost to three-body states (plus the unitarity violating flux loss). Since we have truncated our Hilbert space to remove four-body and higher states, the quantity $r^{(3)J}$ includes only the unitarity-violating contribution. Therefore, a comparison of these ratios with Eq. (3.127) suggests that, for a particular value of J , the framework is *effectively unitary* if the ratio $r^{(3)J}$ is much smaller than both $r^{(1)J}$ and $r^{(2)J}$,

$$r^{(3)J} = \frac{\delta U_{\alpha\alpha}^J(p_0, p_0)}{U_{\alpha\alpha}^{(\text{tot})J}(p_0, p_0)} \ll r^{(1)J}, r^{(2)J}. \quad (3.129)$$

If this is the case, the flux loss to unitarity violating terms is negligible relative to losses to two-body and three-body states.

To show that this accuracy can be achieved in practice, the above ratios for elastic $\pi\pi$ scattering were calculated for driving energy $E = 1400$ MeV in the scalar ($J = 0$) channel, using the dynamical model introduced in Sec. IV. The results are shown in Fig. 12 as functions of the quantity a , where $\epsilon = 10^{-a}$ GeV.

The dashed curve at the top of Fig. 12 is the ratio $r^{(1)0}$. The ratio $r^{(1)0}$ represents the fraction of the elastic $\pi\pi$ scattering flux in the $J = 0$ channel, which is missing from the shadow region, and not appearing as asymptotic one-body states. As discussed above, the ratio $r^{(1)J}$ is identically unity. The dot-dashed curve is $r^{(2)0}$. This represents the fraction of two-pion flux missing from the

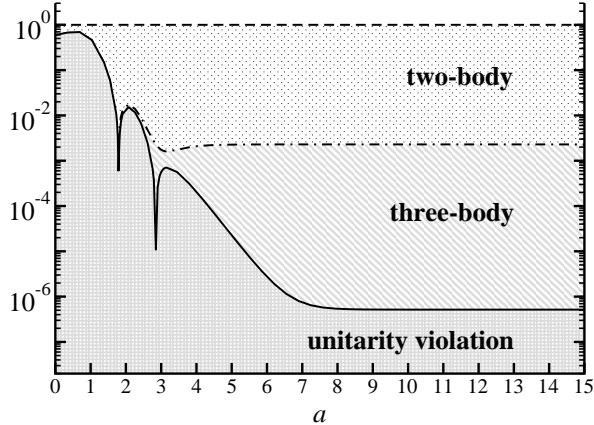


FIG. 12. Fraction of outgoing two-pion flux, at driving energy $E = 1400$ MeV in the scalar ($J = 0$) channel, that appears as “two-body” or “three-body” final states, or is lost to unitarity violations. These fractions are shown versus the exponent a of the adiabatic switching scale $\epsilon = 10^{-a}$ GeV. The curves separating these regions are from Eq. (3.128), and denoted $r^{(1)0} = 1$ (dashed curve), $r^{(2)0}$ (dot-dashed curve), and $r^{(3)0}$ (solid curve).

shadow region that is *not* observed as either asymptotic one- or two-body states. It follows that the region between $r^{(1)0}$ and $r^{(2)0}$, which is labeled “two-body” in Fig. 12, represents the fraction of the flux that appears as asymptotic two-body states. From Fig. 12, one estimates that at $E = 1400$ MeV and with $\epsilon \leq 10^{-4}$ GeV, about 99.8% of the missing $\pi\pi$ flux appears as asymptotic two-body (either, $\pi\pi$ or $K\bar{K}$) states.

The solid curve in Fig. 12 is $r^{(3)0}$. This curve represents the fraction of the two-pion flux missing from the shadow region that is *not* observed as one-, two-, or three-body asymptotic states. The region between $r^{(2)0}$ and $r^{(3)0}$, labeled “three-body” in Fig. 12, represents the fraction appearing as asymptotic three-body states. At energy $E = 1400$ MeV with $\epsilon \leq 10^{-4}$ GeV, one estimates from Fig. 12 that about 0.2% of the missing two-pion flux results in the only open three-body channel $\pi\pi\rho$.

Since the Hilbert space is restricted to one-, two- and three-body states, this should account for all the flux and $r^{(3)0}$ should be identically zero. However in practice, violations to the unitarity condition result in $\delta U_{\pi\pi, \pi\pi}^J(p_0, p_0) \neq 0$. The region below the solid curve is the fraction of the incoming flux that completely disappears from the theory. This region represents the violation to unitarity. For $\epsilon \leq 10^{-7}$ GeV, the violation to unitarity represents a loss of less than 10^{-6} of the outgoing two-pion flux. Therefore, it is completely negligible. It is in this sense that we say the framework employed herein is effectively unitary.

As anticipated, the unitarity violating contribution has one term which is proportional to the adiabatic switching

scale ϵ , and a second term (associated with finite-mesh spacings and numerical inaccuracies) which is independent of ϵ . For the range $10^{-7} < \epsilon < 10^{-2}$ GeV, the violation is linearly proportional to ϵ , while for $\epsilon < 10^{-7}$ GeV, it is roughly constant. This suggests that for $\epsilon \geq 10^{-7}$ GeV, unitarity violation is dominated by the adiabatic switching scale, but when $\epsilon < 10^{-7}$ GeV the violations to unitarity are a result of the numerical errors inherent in our computation methods. That fact that they are so small clearly demonstrates the stability of our numerical methods. In the phenomenological study described in Sec. IV, we used the value $\epsilon = 10^{-12}$ GeV.

IV. APPLICATION TO $\pi\pi$ SCATTERING

In this section, the framework is applied to $\pi\pi$ scattering. Simple model forms of the elementary vertex form factors $V_{\beta_{12}\alpha_1}(q)$ appearing in Eqs. (3.23) and (3.21) are introduced, and solutions for the self-energies $\Pi_{\beta\alpha}(E)$ and $\Sigma_{\beta\alpha}(p, E)$ and scattering amplitudes $t_{\beta\alpha}^{(1)J}(q, p)$, $t_{\beta\alpha}^{(2)J}(q, p)$, and $\tilde{V}_{\beta_{12}\alpha_1}(q)$ are obtained numerically. We discuss several interesting aspects of the obtained solutions. It should be emphasized that the model introduced in Sec. IV A is preliminary and the manner in which the model parameters are fit to the data may be overly simplistic, as it focuses on reproducing only a few observables and therefore does not represent an exhaustive or complete study of the dynamics of $\pi\pi$ scattering. The motivation is to provide a demonstration of the framework and exhibit the features of our model, and its ability to describe the scattering of a system of strongly-coupled particles with emphasis on the multi-particle channel aspect. More complete studies of meson scattering within the present framework will be the subject of future articles.

In Sec. IV A, the dynamical assumptions are discussed along with the model parameters. A detailed list of the states included in the Hilbert space is provided. The model parameters are determined using a simple method to fit experimental data for the $\pi\pi$ isoscalar-scalar phase shift and ρ -meson decay width, using the S -wave phase shifts from Ref. [21]. In Sec. IV B, some aspects of the $f_0(980)$ scalar meson are discussed in terms of a $K\bar{K}$ bound state. In Sec. IV C the resulting phase shifts, inelasticities and cross sections are provided and compared to the data.

A. Dynamical model for $\pi\pi$ scattering

The model is intended to describe the scattering in a range of center-of-momentum (CM) energies from threshold ($E = 2m_\pi \approx 280$ MeV) to about $E = 1400$ MeV. Above 1400 MeV, it is important to include in more detail the effects of the three scalar mesons observed in this region. For this preliminary study, however, we

avoid making strong assumptions concerning these scalar mesons, hence our model will not be accurate in this energy region. In the following, only the isoscalar-scalar ($I = 0, J = 0$) and isovector-vector ($I = 1, J = 1$) channels are considered. The motivation is to explore some of the interesting physical aspects of the present framework and to estimate the importance of including three-body states in such a model of hadron scattering. The assumptions of the dynamical model are summarized below.

Two-body states: For the channels and energies explored herein, it is assumed that $\pi\pi$ scattering is primarily determined by the dynamics arising from the coupling of the $\pi\pi$ and $K\bar{K}$ two-body channels. Hence, $|\pi\pi\rangle$ and $|K\bar{K}\rangle$ are the only two-body channels included in the Hilbert space.

One-body states: It is assumed that the coupling of the $K\bar{K}$ system is strong enough to result in the appearance of a narrow resonance in the scalar-isoscalar channel at $E \approx 980$ MeV. This state is identified with the $J^{PC} = 0^{++}$ $f_0(980)$ meson. Since this scalar meson is presumed to arise from final-state interactions as a quasi-bound $K\bar{K}$ state, it is not part of the free Hilbert space, and there is no bare mass associated with it. Rather, it appears as a pole in the analytically-continued T -matrix. Furthermore, in the limit that the two-body $\pi\pi$ and $K\bar{K}$ channels decouple, this pole moves to the real-energy axis below the two-kaon threshold; that is, it becomes a $K\bar{K}$ bound state in this limit. We note that the identification of the $f_0(980)$ meson as a $K\bar{K}$ molecule is controversial. Although it appears as a molecular state in our model, the “true” nature of the $f_0(980)$ meson remains an open question.

In contrast to the $f_0(980)$ meson, it is assumed that at least one of the scalar resonances observed in the mass region between 1300 and 1700 MeV will be a QCD bound state; that is, a state which arises as a bound state whose constituents are quarks, antiquarks and gluons. Such states do not arise from the meson final-state interactions, they are not bound states of mesons, and hence must be included in the model as *bare* states with bare masses.

Experiments reveal the presence of several resonances in the scalar-isoscalar channel between 1300 and 1700 MeV. A complete study of the $\pi\pi$ scattering system in this energy range requires the inclusion of each of these resonances into the model. However, to simplify the present study, all of these resonances are modeled in terms of a single scalar resonance. The resonance is assumed to have a mass of 1350 MeV, which gives it a mass similar to the lightest of the resonances above kaon threshold, referred to as the $J^{PC} = 0^{++}$ $f_0(1370)$ meson. One ramification of choosing a single scalar resonance to model the effect of all observed resonances in the 1300–1700 MeV region, is in the width of this resonance. In order to fit the model parameters to the $\pi\pi$ phase shifts requires a single effective resonance with a very large width. It is found that the model resonance has a decay width of 805 MeV, which is approximately

TABLE I. Masses and widths of mesons. Masses that are underlined have been fixed to reproduce the accepted values. All other values are obtained from the model calculation. In the present study, the width of the K^* meson was not calculated. All values are given in units of MeV.

	π	K	ρ	K^*	$f_0(1350)$	$f_0(980)$
mass	<u>140</u>	<u>500</u>	<u>770</u>	<u>890</u>	<u>1350</u>	996
width	0	0	150	—	805	46

TABLE II. Isospin coupling constants for kernel $K_{\beta\alpha}(q, p)$ for isoscalar, S -wave ($I = 0, J^{PC} = 0^{++}$) and isovector, P -wave ($I = 1, J^{PC} = 1^{--}$) scattering.

Channel	Exchange	$I = 0, J = 0$	$I = 1, J = 1$
$\pi\pi \leftrightarrow \pi\pi$	$\pi\pi f_0$	1	1
$K\bar{K} \leftrightarrow K\bar{K}$	$K\bar{K} f_0$	1	1
$\pi\pi \leftrightarrow \pi\pi$	$\pi\pi\rho$	-1	-1
$K\bar{K} \leftrightarrow K\bar{K}$	$K\bar{K}\rho$	-1	-1
$\pi\pi \leftrightarrow K\bar{K}$	$\pi K K^*$	$-\sqrt{2}$	-1

the *sum* of the widths of the three observed resonances in this region.

Three-body states: Only three-body states are included that can couple to the $\pi\pi$ or $K\bar{K}$ states through the absorption or emission of the isovector $J^{PC} = 1^{--}$ $\rho(770)$, isodoublet $J^P = 1^-$ $K^*(892)$, and $J^{PC} = 0^{++}$ f_0 mesons. Thus, the three-body states included in this study are $|\pi\pi\rho\rangle$, $|\pi\pi f_0\rangle$, $|K\bar{K}\rho\rangle$, $|K\bar{K} f_0\rangle$, $|\pi\bar{K} K^*\rangle$ and $|\pi K K^*\rangle$.

To summarize, the hadronic states included in this model of $\pi\pi$ scattering are

$$\begin{aligned}
&|f_0\rangle, |\rho\rangle, \\
&|\pi\pi\rangle, |K\bar{K}\rangle, \\
&|\pi\pi\rho\rangle, |K\bar{K}\rho\rangle, |\pi\bar{K} K^*\rangle, |\pi\pi f_0\rangle, |K\bar{K} f_0\rangle, \quad (4.1)
\end{aligned}$$

where the f_0 meson refers to the $f_0(1350)$ meson. (The $f_0(980)$ meson is expected to appear in the model as a $K\bar{K}$ resonance.) The values of the bare masses of these particles are provided in Table I and are underlined to indicate that they are input parameters. As discussed in Sec. II, one- and two-body counter terms are included in the elementary interaction potentials V_{11} and V_{22} , respectively, such that the bare masses given in Table I coincide with the dressed masses of the mesons.

Model vertex form factors: The vertices in the model are assumed to be finite-sized and hence require the appropriate form factors. They are given by the universal form:

$$V_{\beta_1\beta_2\alpha_1}(q) = a_{\beta_1\beta_2\alpha_1} \sqrt{\frac{16\pi}{2s_{\max} + 1}} e^{-q^2/\Lambda_{\beta_1\beta_2\alpha_1}^2}, \quad (4.2)$$

where $s_{\max} = \max\{s_{\beta_1}, s_{\beta_2}, s_{\alpha_1}\}$ is the largest spin of the particles involved. In the present study $s = 0$ for vertices involving the f_0 meson, and $s = 1$ for vertices involving the ρ or K^* mesons. The vertex coupling constants $a_{\beta_1\beta_2\alpha_1}$ and form factor momentum scales $\Lambda_{\beta_1\beta_2\alpha_1}$ are

TABLE III. Coupling strengths and widths for the vertex form factors. The values of the widths are given in MeV.

$\beta_1\beta_2\alpha_1$	$\pi\pi f_0$	$K\bar{K}f_0$	$\pi\pi\rho$	$K\bar{K}\rho$	$K\pi K^*$
$a_{\beta_1\beta_2\alpha_1}$	12.4	5.08	20.0	20.0	20.0
$\Lambda_{\beta_1\beta_2\alpha_1}$	875	875	875	875	875

chosen to provide a good fit to the data for the isoscalar-scalar $\pi\pi$ phase shift $\delta_{\pi\pi}$ and the ρ -meson decay width $\Gamma_{\rho\rightarrow\pi\pi} = 150$ MeV. The isospin factors that arise in a calculation of the meson-exchange kernels $K_{\beta\alpha}^J(q, p)$, such as in Eq. (3.75), are given in Table II.

Direct interactions: In addition to meson exchanges, it is important to include real-valued potentials that directly couple two pseudoscalar mesons to two pseudoscalar mesons, as a part of the $K^{(4pt)}$ kernel in Eq. (3.65). Such interaction potentials could arise from the direct coupling of four mesons to a virtual-quark loop. Here, two direct four-point interactions are considered. The first is intended as a way to mimic some of the effects of dynamical chiral symmetry breaking. This interaction is taken to be of the form given by the elementary potential V_{22} and is referred to as the direct 4π (or $4K$) interaction. In a partial-wave basis, the form of the four-pion interaction is given by

$$K_{\pi\pi,\pi\pi}^{(4\pi)J}(q, p) = 16\pi (qp)^J a_{4\pi}^2 e^{-q^2/\Lambda_{4\pi}^2} e^{-p^2/\Lambda_{4\pi}^2}, \quad (4.3)$$

and the four-kaon term $K^{(4K)J}(q, p) = 0$. The second four-point interaction is a short-ranged attraction modeled as a t -channel exchange of a heavy scalar-isoscalar meson. Its form is given by the scalar-exchange kernel of Eq. (3.75) and the two-body self-energy Σ of Eqs. (3.36) and (3.37). For simplicity it is treated exactly as if two additional three-body states,

$$|\pi\pi X\rangle, |K\bar{K} X\rangle, \quad (4.4)$$

with $m_X = 1500$ MeV, were added to the Hilbert space. Clearly, modelled in this manner, for energies $E > m_X + 2m_\pi = 1780$ MeV, the state $|\pi\pi X\rangle$ can go on-energy-shell. However, the calculations described herein are for energies less than 1400 MeV, so that $|\pi\pi X\rangle$ is never on-energy-shell.

We stress again that our goal is to study the framework developed in this paper. In particular, we are interested in verifying the possibility of including the dynamics of three-body intermediate states to meson scattering, rather than testing a particular model for the underlying meson-meson interactions in $\pi\pi$ scattering.

Once the forms of the model vertices are fixed, the only observables used in the fit are the scalar-isoscalar $\pi\pi$ phase shift $\delta_{\pi\pi}$, the existence of the $K\bar{K}$ resonance (referred to as the $f_0(980)$), and the decay width of the $\rho(770)$ vector meson. We do not fit all measured reaction channels, since this paper represents more a proof of principle of our framework than a complete phenomenological analysis of $\pi\pi$ scattering. The resulting values of the coupling constants are provided in Tables III and IV.

TABLE IV. Coupling strengths and widths for the four-point meson interactions. The values of the widths are given in MeV.

	$\pi\pi X$	$K\bar{K} X$	4π	$4K$
a	19.8	11.0	17.2	0.0
Λ	1000	1000	750	750

B. The $K\bar{K}$ bound state

In the above procedure, the strength $a_{K\bar{K}X}$ of the attractive, direct coupling of four kaons was chosen to ensure the existence of a $K\bar{K}$ bound state, the $f_0(980)$. In the absence of the two-pion channel, the bound state coincides with the appearance of a pole in the real part of the scattering amplitude $t_{K\bar{K},K\bar{K}}^{(2)}(0, 0)$. However, when the two-pion channel is allowed to mix with the $K\bar{K}$ channel, the $K\bar{K}$ bound state develops a width due to its allowed decay into two pions. If the coupling between the two-pion and two-kaon channels is weak (as it is in the present case), the scattering amplitude takes on a simple Breit-Wigner form

$$\text{Re} t_{K\bar{K},K\bar{K}}^{(2)}(0, 0) \propto \frac{E - m_{f_0(980)}}{(E - m_{f_0(980)})^2 + \Gamma_{f_0(980)}^2/4}, \quad (4.5)$$

near the mass $m_{f_0(980)}$ of the s -channel resonance. A plot of this amplitude versus the CM energy E is depicted as a solid curve in Fig. 13 for the parameters and states considered in this model application, as defined above in Tables I, III, and IV.

We observe that the real part of the amplitude exhibits a narrow, resonance-like behavior just below the $K\bar{K}$ threshold. This is indicative of a one-body intermediate state in that channel. As no such bare state has a mass in this vicinity, the resonance has been dynamically generated from the meson-meson interactions. Its finite width is clearly seen in Fig. 13, and is due to the mixing of the $K\bar{K}$ and $\pi\pi$ channels. This provides a means for the $f_0(980)$ to decay into the $\pi\pi$ state, rendering it unstable.

If the interaction in the $K\bar{K}$ channel is weakened, the bound state $f_0(980)$ disappears. To demonstrate this, the value of the four-point kaon scattering potential is decreased to $a_{K\bar{K}X} = 8.5$. With this value of the coupling strength, the K and \bar{K} mesons do not bind and there is no $f_0(980)$ resonance observed in the model. The real part of $t_{K\bar{K},K\bar{K}}^{(2)}(0, 0)$ that results is depicted as the dashed curve in Fig. 13. There is no resonance-like behavior in this amplitude. However, one can now clearly observe the cusp in the dashed curve at $E = 2m_K = 1000$ MeV, which is indicative of the opening of the $K\bar{K}$ two-body threshold.

The cusp, apparent in the dashed curve in Fig. 13, arises from a discontinuity in the first derivative of $t_{K\bar{K},K\bar{K}}^{(2)J=0}(0, 0)$ with respect to E , at the kaon threshold

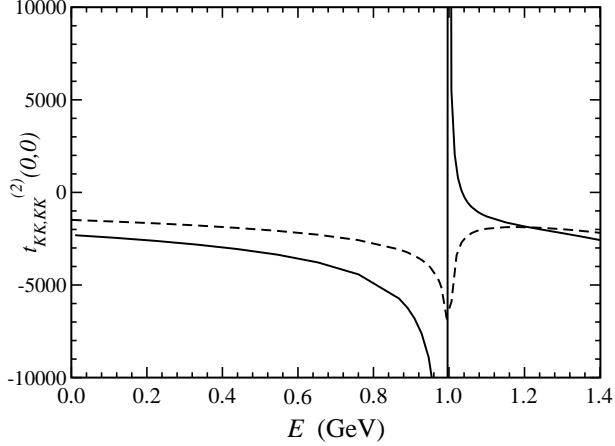


FIG. 13. Plot of the real part of $t_{K\bar{K} \leftarrow K\bar{K}}^{(2)J=0}(q, p)$ versus the CM energy E with $q = p = 0$. The solid curve results from the model calculation using parameters from Tables I—III. The dashed curve results from a calculation that uses the same values except a smaller value of $a_{K\bar{K}X} = 8.5$. This weakens the attraction between the two kaons such that they fail to form a bound state, and consequently the $f_0(980)$ meson vanishes from the model.

at $E = 1000$ MeV. The $K\bar{K}$ threshold appears in the S -wave, from which it follows that although $t_{\beta\alpha}^{(2)J=0}(0, 0)$ is a continuous function of E , its first derivative is not well-defined at the two-kaon threshold.

The analytic behavior of $t_{\beta\alpha}^{(2)J}(0, 0)$ provides an excellent *theoretical* indicator for the appearance of bound states. It provides a clear signal even when bound states appear nearly on top of a two- or three-body threshold, such as the case depicted in Fig. 13. The reason is that the analytic behavior of a one-body resonance is sufficiently different from that of two- and three-body states to provide a clear distinction between them.

C. Phase shifts and inelasticities

Below all three-body thresholds, the non-trivial part of the S -matrix in Eq. (2.17) can be written as a 2×2 unitary matrix $S_{\beta\alpha}(E)$ with α, β denoting the only two open channels $\pi\pi$ and $K\bar{K}$. The S -matrix in the J^{th} partial wave can be parametrized in terms of two phase shifts $\delta_{\pi\pi}$ and $\delta_{K\bar{K}}$, and one inelasticity $\eta_{\pi\pi}$,

$$S_{\beta\alpha}^J(E) = \begin{pmatrix} \eta_{\pi\pi} e^{2i\delta_{\pi\pi}} & i\sqrt{1-\eta_{\pi\pi}^2} e^{i(\delta_{\pi\pi}+\delta_{K\bar{K}})} \\ i\sqrt{1-\eta_{\pi\pi}^2} e^{i(\delta_{\pi\pi}+\delta_{K\bar{K}})} & \eta_{\pi\pi} e^{2i\delta_{K\bar{K}}} \end{pmatrix}, \quad (4.6)$$

for $\alpha = |\pi\pi\rangle, |K\bar{K}\rangle$. Herein, the phase shifts $\delta_{\pi\pi}$ and $\delta_{K\bar{K}}$ and the two inelasticities $\eta_{\pi\pi}$ and $\eta_{K\bar{K}}$ are defined by

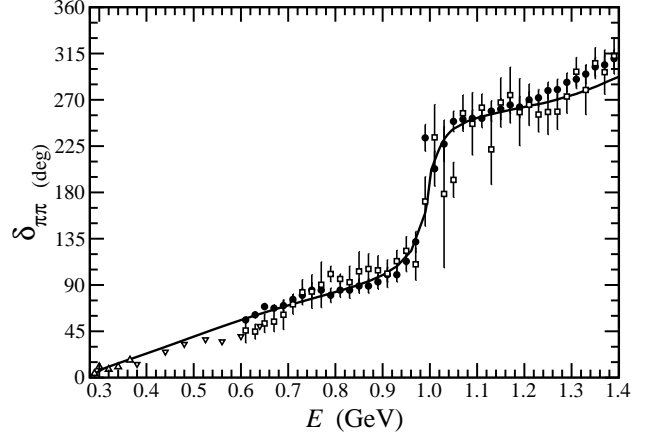


FIG. 14. The $\pi\pi$ scattering phase $\delta_{\pi\pi}$ in the scalar, isoscalar channel as a function of the CM driving energy E . The data are from Refs. [22] (open squares), [23] (closed circles), [24] (up triangles), and [25] (down triangles).

$$\delta_{\alpha}(E) = \frac{-i}{2} \ln \frac{S_{\alpha\alpha}^J(E)}{\eta_{\alpha}(E)}, \quad (4.7)$$

$$\eta_{\alpha}(E) = |S_{\alpha\alpha}^J(E)|. \quad (4.8)$$

Below all three-body thresholds there are only two stable channels, $\pi\pi$ and $K\bar{K}$. Hence, there is only one inelasticity parameter $\eta_{\pi\pi} = \eta_{K\bar{K}}$. For energies E above the lowest stable three-body threshold, one must augment the S -matrix of Eq. (4.6) by including all stable three-body states. Consequently, its parametrization requires more than two phase shifts and one inelasticity. Nonetheless, one may still use Eqs. (4.7) and (4.8) to define the phase shifts $\delta_{\alpha}(E)$, and inelasticities $\eta_{\alpha}(E)$ for the two channels $\alpha = \pi\pi$ and $K\bar{K}$. Of course, above the threshold of a stable three-body state $\eta_{\pi\pi} \neq \eta_{K\bar{K}}$.

The $\pi\pi$ phase shift, as defined by Eq. (4.7) and obtained from our model, is shown as a solid curve in Fig. 14. The model provides an excellent description of the $\pi\pi$ phase shift data depicted in Fig. 14 [22–25], and the inelasticity $\eta_{\pi\pi}$, as shown in Fig. 15. The overall trend of the pion scattering phase shift $\delta_{\pi\pi}$ is positive and increases slowly with energy E . This is indicative of a weak and attractive effective $\pi\pi$ scattering potential. At the kaon threshold, a rapid phase motion is apparent. It results from the presence of a narrow, $f_0(980)$ scalar meson. Above the two-kaon threshold, the phase shift continues to increase slowly, at a rate similar to the increase in the phase shift below the threshold.

Below all other thresholds, the $\pi\pi$ channel is the only open channel, and unitarity requires that the inelasticity $\eta_{\pi\pi} = 1$ here. This is clearly observed in Fig. 15, where the calculated inelasticity $\eta_{\pi\pi}$ has a value consistent with unity below the threshold of the $K\bar{K}$ channel at 1 GeV. Had four-body states been included into this framework, one might have expected to see a decrease in

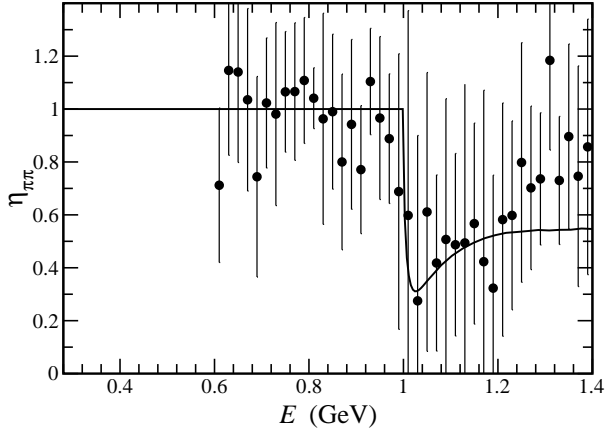


FIG. 15. The $\pi\pi$ scattering inelasticity $\eta_{\pi\pi}$ in the scalar, isoscalar channel as a function of the CM driving energy E . The data are from Ref. [22].

the inelasticity $\eta_{\pi\pi}$ due to the opening of the four-pion state, which has a threshold of $E = 4m_\pi \approx 0.560$ GeV. However, the data in Fig. 15 [22] seem to suggest that the contribution of the four-pion state to $\pi\pi$ scattering is negligible. This can be seen by noting the lack of any systematic deviation from $\eta_{\pi\pi} = 1$ for the range of energies $4m_\pi < E < 2m_K$.

It is clear from both Figs. 14 and 15 that the $K\bar{K}$ channel has a significant effect on $\pi\pi$ scattering. At the two-kaon threshold at $E = 1.0$ GeV, one observes a rapid increase in the $\pi\pi$ phase shift $\delta_{\pi\pi}$, and a sharp fall off of the $\pi\pi$ inelasticity $\eta_{\pi\pi}$ to its minimum value $\eta_{\pi\pi} \approx 0.31$. This phase motion is indicative of crossing the thresholds of the two-body $K\bar{K}$ state and the one-body $f_0(980)$ bound state. The rapid increase observed in the phase shift $\delta_{\pi\pi}(E)$ is due to the *weak* coupling between the $\pi\pi$ and $K\bar{K}$ channels. In the model, when the mixing of these two channels is further weakened, the rate of change of the phase motion tends to *increase*, until finally, in the limit that the coupling between the two channels goes to zero, the phase motion becomes a step-function of magnitude 180 degrees. Such a phase motion is completely unobservable, and could therefore be ignored altogether (although it is relevant to Levinson's theorem, which relates overall changes in the phase shifts from threshold to infinite energy to the number of bound states in a system).

The importance of the coupling between the two-body channels $\pi\pi$ and $K\bar{K}$ can be estimated quantitatively by recalculating the pion phase shift $\delta_{\pi\pi}$ after removing the kaon state $|K\bar{K}\rangle$ from the Hilbert space. The result is shown as the dotted curve in Fig. 16. However, from the above argument, perhaps a better indication of the importance of the $K\bar{K}$ channel is obtained by letting the couplings that lead to a mixing between the $K\bar{K}$ and $\pi\pi$ channels go *smoothly* to zero. (In practice,

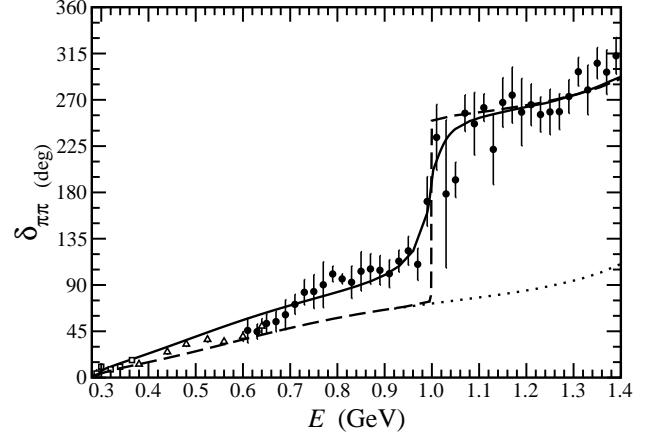


FIG. 16. The $\pi\pi$ scattering phase $\delta_{\pi\pi}$ in the scalar, isoscalar channel versus the CM energy E . The full calculation (solid curve) is compared to the calculation (dashed and dotted curves) in the limit the $K\bar{K}$ and $\pi\pi$ states become decoupled. The data are from Ref. [22].

this is done by not allowing the one-body scalar $f_0(1350)$ to have a bare coupling to the $K\bar{K}$ state, and setting $a_{K^*\pi K} = 0$. This has a minimal effect on the dynamics but prevents mixing the $|\pi\pi\rangle$ and $|K\bar{K}\rangle$ states.) In this limiting case, the two states $|K\bar{K}\rangle$ and $|f_0(980)\rangle$ are coupled to the $|\pi\pi\rangle$ state, but the contributions they make to $\pi\pi$ scattering go to zero. The result is that for energies $E > 1000$ MeV, the $\pi\pi$ scattering amplitude will cross the branch cuts associated with the opening of these two channels. But since these channels do not mix with the $\pi\pi$ channel in this limit, the $\pi\pi$ phase shift exhibits a step-like motion at $E = 1.0$ GeV. This is shown as the dashed curve in Fig. 16. The difference between the solid curve, which represents the full model calculation, and the dashed curve in Fig. 16 may be taken as being indicative of the significance of the $K\bar{K}$ channel on $\pi\pi$ scattering. We conclude that the mixing between the $\pi\pi$ and $K\bar{K}$ channels is significant near and below the two-kaon threshold, where it can contribute more than half of the total phase shift $\delta_{\pi\pi}$. At energies above the two-kaon threshold, its importance quickly diminishes and vanishes altogether above $E = 1150$ MeV.

The importance of the mixing between the $\pi\pi$ and $K\bar{K}$ channels can also be observed in the pion inelasticity $\eta_{\pi\pi}$ shown in Fig. 15. Just above the two kaon threshold, the inelasticity plummets to a minimum value $\eta_{\pi\pi} \approx 0.31$. In the limit that the coupling to the kaon channel goes to zero, as described above, the inelasticity takes on a very different appearance.

In Fig. 17, the two pion inelasticity is plotted above the $K\bar{K}$ threshold. Below the threshold its value is unity. The lowest multi-particle state to which two-pion flux can be lost is the three-particle channel $|\pi\pi\rho\rangle$. The production threshold of this state is 1050 MeV. We observe

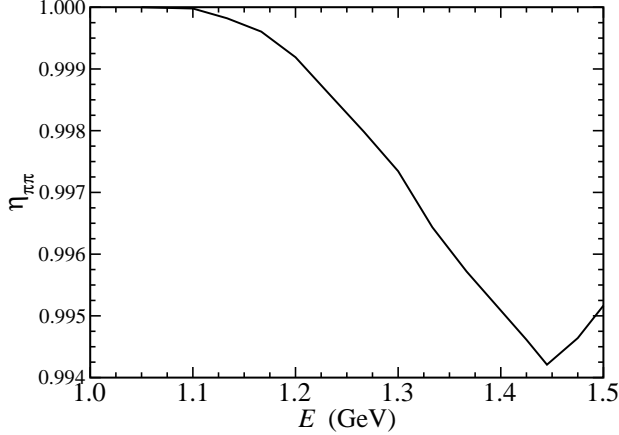


FIG. 17. The $\pi\pi$ inelasticity $\eta_{\pi\pi}$ in the isoscalar-scalar channel with no kaons.

a slow decrease in the inelasticity $\eta_{\pi\pi}$ above 1050 MeV, due to the opening of the $\pi\pi\rho$ channel. The effect of this channel on the inelasticity is very small, with a minimum value $\eta_{\pi\pi} \approx 0.994$.

The energy dependence of the S -wave pion scattering inelasticity $\eta_{\pi\pi}$ and phase shift $\delta_{\pi\pi}$ are conveniently plotted together in an Argand diagram. In Fig. 18, the partial-wave scattering amplitude $a_{\pi\pi}^{J=0}(E)$ is plotted in the complex plane as a parametric function of the CM energy E . This figure clearly shows the rapid rise in the elastic $\pi\pi$ phase shift just below 1 GeV, and the resulting dramatic loss of flux from the elastic channel as soon as the $K\bar{K}$ channel opens up.

For spinless particles, the amplitude is given by

$$\begin{aligned} a_{\pi\pi}^J(E) &= \frac{\eta_{\pi\pi} e^{2i\delta_{\pi\pi}} - 1}{2i}, \\ &= -\frac{p_0}{(4\pi)^2} \frac{1}{2E} z_{\pi\pi} \\ &\quad \times \left(t_{\pi\pi, \pi\pi}^{(1)J}(p_0, p_0) + t_{\pi\pi, \pi\pi}^{(2)J}(p_0, p_0) \right), \end{aligned} \quad (4.10)$$

where $p_0 = \sqrt{E^2/4 - m_{\pi}^2}$ is the magnitude of the on-energy-shell three-momentum of the pions, $z_{\pi\pi}$ is the wave function renormalization of the two-pion state $|\pi\pi\rangle$, and $t_{\beta\alpha}^{(1)J}(q, p)$ and $t_{\beta\alpha}^{(2)J}(q, p)$ are the two-body scattering amplitudes, obtained from Eqs. (3.87) and (3.100), respectively. The two-body scattering cross section $\sigma_{\beta\leftarrow\alpha}(E)$ can be written in terms of the partial-wave scattering cross sections according to

$$\sigma_{\beta\leftarrow\alpha}(E) = \sum_{J=0}^{\infty} \sigma_{\beta\leftarrow\alpha}^J(E). \quad (4.11)$$

In terms of our scattering amplitudes, these partial-wave cross sections are given by

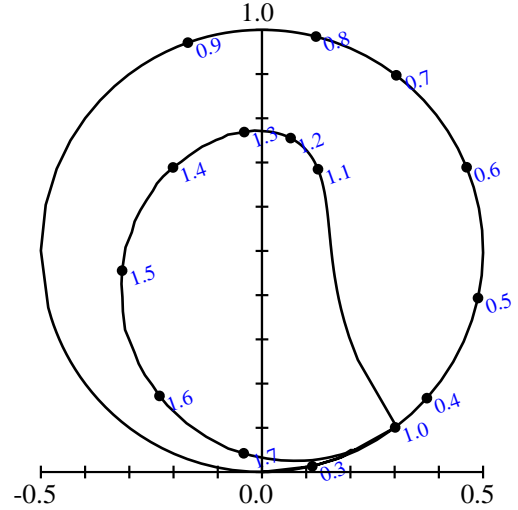


FIG. 18. Argand diagram for $\pi\pi$ scattering at all energies. Plotted is the energy dependence of the real and imaginary parts of the partial-wave scattering amplitude $a_{\pi\pi}^{J=0}(E)$ for the $J = 0$ partial wave from Eq. (4.9) or Eq. (4.10). The curve is calculated for all energies $E > 2m_{\pi}$, and annotated with the corresponding energies E in GeV, from threshold to above $E = 1.7$ GeV.

$$\begin{aligned} \sigma_{\beta\leftarrow\alpha}^J(E) &= \\ &= \frac{2J+1}{4\pi} \frac{z_{\beta} z_{\alpha}}{64\pi^2 E^2} \left| t_{\beta\alpha}^{(1)J}(q_0, p_0) + t_{\beta\alpha}^{(2)J}(q_0, p_0) \right|^2, \end{aligned} \quad (4.12)$$

where p_0 and q_0 are the on-energy-shell solutions to $\mathcal{M}_{\alpha}(p_0) = E$ and $\mathcal{M}_{\beta}(q_0) = E$, respectively. The resulting cross section for elastic, S -wave $\pi\pi$ scattering is shown as a solid curve in Fig. 19. It is finite at threshold, exhibits a maximum value of 43 millibarns at $E \approx 600$ MeV, and a sharp decrease at the position of the $f_0(980)$ scalar meson resonance. This sudden drop occurs just below the $K\bar{K}$ threshold, as can be seen upon examination of the inset plot in Fig. 19 which depicts a closeup of the $K\bar{K}$ threshold region.

The dot-dashed curve is the resulting cross section $\sigma_{K\bar{K}\leftarrow\pi\pi}^{J=0}$ for the two-kaon production process $\pi\pi \rightarrow K\bar{K}$. This cross section is considerably smaller than that of the elastic $\pi\pi$ scattering cross section, reaching its maximum value of 4.6 millibarns just above the two-kaon threshold at $E = 1$ GeV. Its small size is a result of the weak coupling between the two-pion and two-kaon channels. As discussed above, a weak coupling of these channels is necessary to ensure a narrow $f_0(980)$ meson. If the mixing between the pion and kaon channels were stronger, the $f_0(980)$ meson would more easily decay into two pions, tending to increase its width significantly.

The dashed curve in Fig. 19 is the S -wave cross section for elastic $K\bar{K}$ scattering. This cross section is comparably huge, having its maximum at the two-kaon threshold energy. Its size can be compared to that of the two-pion elastic cross section,

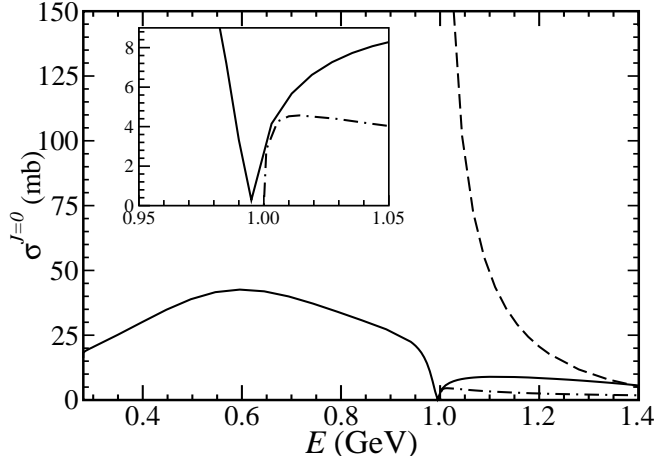


FIG. 19. S -wave cross section $\sigma^{J=0}(E)$ in millibarns for $\pi\pi \rightarrow \pi\pi$ (solid curve), $K\bar{K} \rightarrow K\bar{K}$ (dashed curve), and $\pi\pi \rightarrow K\bar{K}$ (dot-dashed curve). The inset shows a detail of the region around the $K\bar{K}$ threshold at $E = 1$ GeV.

$$\begin{aligned}\sigma_{\pi\pi \leftarrow \pi\pi}^{J=0}(E = 2m_\pi) &\approx 18.3 \text{ mb}, \\ \sigma_{K\bar{K} \leftarrow K\bar{K}}^{J=0}(E = 2m_K) &\approx 734 \text{ mb}.\end{aligned}$$

The very large $K\bar{K}$ cross section arises from the scalar $f_0(980)$ meson which lies just below the $K\bar{K}$. The presence of a bound state just below the two-body scattering threshold will generally tend to increase the size of the cross section dramatically.

As was discussed earlier in Sec. IV A, the model parameters were chosen to provide a good fit to the S -wave pion phase shift $\delta_{\pi\pi}$ data from Ref. [21]. In Fig. 14, we observe that the resulting phase shifts are also in excellent agreement with the data analyses of Ref. [22], [24], and [25]. However, it is important to realize that direct comparison of our model results with these $\pi\pi$ scattering data must be done with caution. Extraction of these data requires the use of theoretical models, or theoretical assumptions, in order to fit the experimental observables. In the worst-case scenario, the resulting $\pi\pi$ phase shift data may be more representative of the extraction methods employed than of the actual $\pi\pi$ scattering process.

The extraction of the $\pi\pi$ phase shifts from experiment is a difficult and long-standing problem of hadron physics. At present, it is impossible to construct an experiment in which a pion beam is scattered from a pion target. Hence, other techniques are required to extract the $\pi\pi$ phase shift from experimental observables. One possibility is to use decays that produce two pions in the final state, and attempt to extract the $\pi\pi$ phase shifts from the final-state interactions.

The procedure employed by Ref. [24] is extract the phase shifts from the electroweak kaon decay $K^+ \rightarrow \pi^+\pi^0 e^+\nu_e$. The results are shown as open squares in Figs. 17 and 20. Extraction of the phase shift using de-

cays with more than two particles in the final state requires some knowledge of transition form factors for the coupling of a kaon, two pions and the W boson to determine $K^+ \rightarrow \pi^+\pi^-W^+$. A nice feature of employing the electroweak decay $K^+ \rightarrow \pi^+\pi^0 e^+\nu_e$ is that the two pions are the only strongly-interacting particles in the final state. Hence, one would expect that the $\pi\pi$ interactions would be the dominant contribution to the dressing of the final state. However, this approach is hampered by two experimental difficulties. The first is the lack of statistics. This particular kaon decay represents only a small fraction (4×10^{-5}) of the total K^+ -meson decay width, which is already extremely small. The second is the fact that the energies and angles of the outgoing leptons provide a small lever arm with which to vary the CM energy E of the two final-state pions.

Another method is to extract the final state interactions of the two-pion production process $\pi p \rightarrow \pi\pi n$, employed by Ref. [25] (down triangles), Ref. [22] (open squares), and Ref. [23] (closed circles), shown in Fig. 14. These studies require some theoretical input in order to perform the extraction of the $\pi\pi$ scattering phase shift $\delta_{\pi\pi}$ and inelasticity $\eta_{\pi\pi}$; hence, they are not direct measurements of the $\pi\pi$ scattering phase shift.

Our model parameters were originally fit to the $\pi\pi$ phase shifts obtained by an analysis [23] of an experiment at CERN involving $\pi^- p \rightarrow \pi^+\pi^- n$ at 17.2 GeV. Recently, this same data was re-examined by Kaminski *et al.* [22], with weaker model assumptions than were used in Ref. [23]. The work of Ref. [22] provides an exhaustive and *nearly* complete study of the $\pi\pi$ phase shift. In particular, there is no assumption that pion exchange is the dominant mechanism for the process $\pi^- p \rightarrow \pi^+\pi^- n$. Consequently, we believe this analysis to be more general than any other. A relative phase ambiguity in the analysis of Ref. [22] provides four possible, distinct solutions for the $\pi\pi$ phase shifts and inelasticities. Two of these solutions seem to have an unphysical inelasticity $\eta_{\pi\pi}$ below the two-kaon threshold and can be discarded. The other two solutions, denoted the “up-flat” and “down-flat” solutions, are very similar in appearance and cannot be dismissed on qualitative grounds. The phase shifts from the “down-flat” solution of Ref. [22] are shown as solid circles in Figs. 16 and 20.

The general behavior of the $\pi\pi$ phase shift $\delta_{\pi\pi}$ is positive, which is indicative of an attractive $\pi\pi$ scattering amplitude. An abrupt increase in the pion phase shift is evident at 1 GeV, which is due to the combined effects of the opening of the $K\bar{K}$ threshold and the crossing of the scalar $f_0(980)$ resonance.

Apart from this feature, which in our model results from the delicate mixing between the $\pi\pi$ and $K\bar{K}$ channels, the calculated pion phase shift $\delta_{\pi\pi}$ exhibits a steady, gentle increase from the threshold at 280 MeV to above 1400 MeV! In our model, this slowly increasing behavior arises from subtle cancellations between the attractive potentials of the heavy scalar-meson exchanges and the repulsive, direct four-pion interaction from Eq. (4.3)

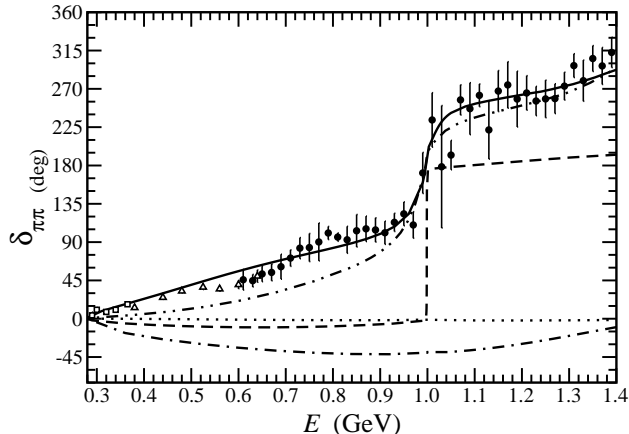


FIG. 20. Importance of the different model contributions to $\pi\pi$ scattering phase shift. The solid curve is the full calculation. The dashed curve is obtained by removing the one-body state $f_0(1350)$ from the Hilbert space. The dot-dashed curve is obtained by completely removing the scalar $f_0(1350)$ from the theory, both in one-body and three-body states. The dotted curve is same as the dot-dashed curve, but all scalar couplings (the “X”-exchanges and contact terms) are also set to zero. This is the effect of just the vector-meson exchanges. Above threshold it is negative with a minimum of $\delta_{\pi\pi} \approx -2.0$ degrees at $E \approx 1.2$ GeV. The dot-dot-dashed curve is obtained by weakening the coupling of the one-body $f_0(1350)$ state to the $\pi\pi$ state by 10 percent. The data points are from Fig. 14.

which is intended to model the effect dynamical chiral symmetry breaking. The different form factor scales involved in these interactions (see Tables III and IV) are chosen to provide this slowly increasing, weak phase shift observed in the two-pion channel. Typically, scalar potentials by themselves provide a strong attraction in the S -wave $\pi\pi$ channel, that leads to a rapidly rising phase shift just above the $\pi\pi$ threshold, which then quickly falls away. This behavior is not seen in the $\pi\pi$ phase shift $\delta_{\pi\pi}$.

The importance and role of the scalar resonances in $\pi\pi$ scattering can be appreciated by a close examination of Fig. 20. The effect of the heavy s -channel resonances which are collectively modeled by the single $f_0(1350)$ in our model is two fold. First, their presence leads to a strong attractive potential for energies below 1400 MeV. Second, they provide the most important contribution to *off-diagonal* matrix elements of the two-body scattering kernel K . That is, they provide the strongest source of mixing for the two-pion and two-kaon states in this model.

Both of these effects tend to produce an attraction for the two pions. In particular, the strong attraction necessary to bind the kaons to form the $f_0(980)$ resonance results in a strong attraction in the two-pion channel as well. The amount of mixing between the two-pion and

two-kaon states dictates the attraction felt by the pions. Hence, when the coupling between $|\pi\pi\rangle$ and $|f_0(1350)\rangle$ states is artificially reduced by as little as 10%, the result is significant, as shown by the dot-dot-dashed curve in Fig. 20. When the one-body state $|f_0(1350)\rangle$ is removed entirely from the Hilbert space, the result is the dashed curve. The resulting pion phase shift is negative and close to zero below the two-kaon threshold, and positive above the threshold. The absence of the one-body s -channel state $f_0(1350)$ reduces the mixing between the two-pion and two-kaon states, which results in a nearly stable (and very narrow) kaon bound state $f_0(980)$. In this case, we observe a $f_0(980)$ bound states with a width that is reduced from 46 MeV to 0.28 MeV! This is a result of the fact that the $f_0 \rightarrow \pi\pi$ decay must proceed through K^* exchange in the kernel K , which provides only a weak mixing of the $\pi\pi$ and $K\bar{K}$ states.

When all scalar mesons are removed from the theory entirely; that is, when the couplings that lead to the existence of one-body states $|f_0(1350)\rangle$, and three-body states $|f_0\pi\pi\rangle$ and $|f_0K\bar{K}\rangle$ are set to zero $a_{\pi\pi f_0} = a_{K\bar{K}f_0} = 0$, the resulting phase shift is shown in Fig. 20 by the dot-dashed curve. The slightly repulsive behavior is a result of the combined effect of the attractive scalar- X and repulsive four-point interactions associated with chiral symmetry, given by the parameters in Table IV.

To minimize the number of free parameters all of the couplings to vector mesons are chosen to be equal to each other,

$$a_{\pi\pi\rho} = a_{K\bar{K}\rho} = a_{\pi K K^*}. \quad (4.13)$$

These coupling strengths were then determined by solving P -wave $\pi\pi$ scattering at the ρ meson mass $E = m_\rho = 770$ MeV, and requiring that the ρ -meson width reproduced the experimental value $\Gamma_\rho = 150$ MeV, as given in Table I. We find that the resulting coupling strength leads to a vector-meson exchange interaction kernel K which provides a very weak repulsion for $\pi\pi$ scattering. This is illustrated by the dotted curve in Fig. 20, where we have set all of the couplings except those involving the vector mesons ($a_{\rho\pi\pi}$, $a_{\rho K\bar{K}}$, $a_{K^*\pi\bar{K}}$) to zero. The resulting phase shift is negative (repulsive) and very small; its largest absolute value is about 2 degrees. Thus, in this model, ρ -meson exchange is negligible in the S wave. This model differs from the analysis of Ref. [14], in which they report that the attractive potential (which leads to the binding of the $K\bar{K}$ into the $f_0(980)$ resonance) is primarily due to ρ -meson exchange, which is strong and attractive in their model. In our framework, we find that the exchange of a spin-1 meson in the kernel K results in a very weak and mildly repulsive interaction. This difference is a result of how the spin couplings and energy denominators of the meson-exchange propagators are implemented in the kernels of the two frameworks.

V. SUMMARY AND FUTURE DIRECTIONS

We have formulated a framework suitable for the description of nonperturbative hadron scattering, based on the Bakamjian-Thomas formulation of relativistic quantum mechanics. In Sec. II, it is shown that by including the interactions into the free mass operator \mathcal{M} , one can ensure that observables calculated in the framework are Lorentz covariant. When the Hilbert space is truncated to contain only one-, two- and three-body states, the resulting Lippmann-Schwinger equations (LSEs) form a closed set of coupled integral equations. The solution of these integral equations is obtained numerically.

A significant improvement of this framework over earlier work is that the *full* effect of three-body states have been included. It is shown in Sec. II, that the three-body Green functions appear only in the two-body scattering kernel K and the two-body self-energy Σ , and that for energies E above the three-body thresholds, unitary branch cuts associated with these thresholds appear both in K and Σ . It follows that the kernel K and two-body self-energy Σ are *complex* functions of the energy E . The appearance of such three-body branch cuts provides the means for important dynamical effects, such as three-hadron production and decays into three-hadron states, which are automatically accounted for in our framework. Such effects have hitherto been ignored for the most part in previous studies.

The inclusion of three-body cuts into our integral equations requires appropriate numerical methods to be employed. These methods, necessary to solve the coupled set of LSEs, are described in Sec. III and shown to maintain the unitarity of the theory to better than one part in one million. To demonstrate the utility of the framework, a preliminary study of $\pi\pi$ scattering is carried out in Sec. IV. The simple model, introduced in Sec. IV A, is able to provide an excellent description of the $\pi\pi$ phase shifts and inelasticities.

The main purpose for developing this framework is to provide a means of incorporating the dynamics of low-momentum transfer, final-state interactions into the study of hadronic processes for energies up to a couple of GeV. In this energy region, the comparison between experimental data and theoretical predictions made using models of QCD for quark and gluon dynamics, are often made difficult due to the presence of final-state interactions. The soft rescattering of final-state hadrons tends to *mask* the QCD dynamics of interest. It is our belief that the framework developed herein provides a tractable means to incorporate the effects of final-state interactions into studies of hadronic phenomena.

Towards this end, the framework is constructed to be a consistent extension for the constituent quark model. It provides a means to *unquench* the quark model by providing for hadron loops, multi-particle thresholds and the unitarity branch cuts associated with these. The result is the generation of complex-valued scattering amplitudes.

It is an extension of the quark model, in that the quark model may be used to provide the elementary couplings and form factors for the hadronic interactions in V . Our framework uses this real potential V to generate the full scattering solution.

Future applications of the framework will focus on the dynamics of nucleon resonances and exotic, hybrid mesons that are the subject of current and proposed experiments at TJNAF. In the baryon case, for energies up to about 2 GeV, there are some well-known and striking examples in πN scattering for which three-body effects are crucial in understanding the experimental observables. For example, in the $L_{2I,2J} = P_{11}$ channel, the πN inelasticity arising from the three-body $\pi\pi N$ state is very large [1]. It is likely that an complete understanding of the P_{11} πN scattering channel and the mysterious $N^*(1440)$ resonance requires the full implementation of three-body unitary cuts that this framework provides.

The effect of three-body cuts in exotic partial waves can also be very important. Most theoretical studies of hybrid meson decays have so far ignored effects of final state interactions. The best candidate for the exotic meson, the $\pi_1(1600)$ [27] was found in the $\rho\pi$ decay channel, which is predicted to be suppressed with respect to other two body decay channels, in particular the $b_1\pi$ [28,29]. This shift of strength from $b_1\pi$ to $\rho\pi$ could be explained by mixing with the three-body, $\omega\pi\pi$ intermediate state which has strong coupling to these two-meson channels.

ACKNOWLEDGMENTS

This work is supported by the U.S. Department of Energy under contract DE-FG02-87ER40365 and the National Science Foundation under contract PHY0070368.

-
- [1] J. A. Johnstone and T.-S. H. Lee, Phys. Rev. **C34**, 243 (1986).
 - [2] R. Jaffe, Phys. Rev. D **15**, 267 (1977).
 - [3] J. Weinstein and N. Isgur, Phys. Rev. D **27**, 588 (1983).
 - [4] T. Barnes, Phys. Lett. **B165**, 434 (1985).
 - [5] D. Morgan and M. R. Pennington, Phys. Lett. **B258**, 444 (1991).
 - [6] J.A. Oller, E. Oset, and J.R. Pelaez, Phys. Rev. Lett. **80**, 3452 (1998).
 - [7] E. Klempt, B.C. Metsch, C.R. Munz, and H.R. Petry, Phys. Lett. **B361**, 160 (1995).
 - [8] N.N. Achasov and G.N. Shestakov, Usp. Fiz. Nauk. **161**, 53 (1991).
 - [9] Particle Data Group, Eur. Phys. J. C **15**, 1 (2000).
 - [10] C. J. Morningstar and M. J. Peardon, Phys. Rev. D **60**, 034509 (1999); G. S. Bali *et al.* [SESAM Collaboration], Nucl. Phys. Proc. Suppl. **53**, 239 (1997)
 - [11] S. Narison, Nucl. Phys. **B509**, 312 (1998)

- [12] P. Minkowski and W. Ochs, Eur. Phys. J. **C9**, 283 (1999)
- [13] R. Kaminski, L. Lesniak, and B. Loiseau, Eur. Phys. J. **C9**, 141 (1999)
- [14] G. Janssen, B.C. Pearce, K. Holinde, and J. Speth, Phys. Rev. **D52**, 2690 (1995).
- [15] R. Kaminski, L. Lesniak, and J.-P. Maillet, Phys. Rev. **D50**, 3145 (1994).
- [16] R. Kaminski, L. Lesniak, B. Loiseau, Phys. Lett. **B413**, 130 (1997).
- [17] B. Bakamjian and L. H. Thomas, Phys. Rev. **92**, 1300 (1953).
- [18] M. Betz and F. Coester, Phys. Rev. **C21**, 2505 (1980).
- [19] M. I. Haftel and F. Tabakin, Nucl. Phys. **158**, 1 (1970).
- [20] C. Moller, Danske Vidensk. Selsk. Mat-Fys. Medd. **23**, 1 (1945).
- [21] B. R. Martin, D. Morgan, and G. Shaw, in “Pion-Pion Interactions in Particle Physics” (Academic, London, 1976), pp. 87-101, and references therein.
- [22] R. Kaminski, L. Lesniak, and K. Rybicki, Acta. Phys. Polon. **B31**, 895 (2000).
- [23] G. Grayer, et al., Nucl. Phys. **B75**, 189 (1974).
- [24] L. Rosselet, et al., Phys. Rev. **D15**, 574 (1977).
- [25] V. Shrinivasan et al., Phys. Rev. **D12**, 681 (1975).
- [26] A.D. Martin and E.N. Ozmütlu, Nucl. Phys. **B158**, 520 (1979).
- [27] G. S. Adams *et al.* [E852 Collaboration], Phys. Rev. Lett. **81**, 5760 (1998).
- [28] N. Isgur, R. Kokoski and J. Paton, Phys. Rev. Lett. **54**, 869 (1985).
- [29] P. Page, E.S. Swanson, and A.P. Szczepaniak, Phys. Rev. **D59**, 034016 (1999).